

# High Resolution Studies of Radio Sources in the Hubble Deep and Flanking Fields

T.W.B. Muxlow<sup>1</sup>, A.M.S. Richards<sup>1</sup>, S.T. Garrington<sup>1</sup>, P.N. Wilkinson<sup>1</sup>,  
B. Anderson<sup>1</sup>, E.A. Richards<sup>2</sup>, D.J. Axon<sup>3</sup>, E.B. Fomalont<sup>4</sup>, K.I. Kellermann<sup>4</sup>,  
R.B. Partridge<sup>5</sup> and R.A. Windhorst<sup>6</sup>

<sup>1</sup>*MERLIN/VLBI National Facility, Jodrell Bank Observatory, University of Manchester, Macclesfield, Cheshire, SK11 9DL, UK.*

<sup>2</sup>*Department of Physics, Talladega College, Talladega, Alabama 35160, USA*

<sup>3</sup>*Department of Physics, Rochester Institute of Technology, 84 Lomb Memorial Drive, Rochester, NY 14623, USA.*

<sup>4</sup>*NRAO Edgemont Road, Charlottesville, Virginia 22903, USA.*

<sup>5</sup>*Department of Astronomy, Haverford College, Haverford, PA 19041, USA.*

<sup>6</sup>*Department of Physics and Astronomy, Arizona State University, Box 871504, Tempe, AZ 85287-1504, USA.*

17 June 2018

## ABSTRACT

Eighteen days of MERLIN data and 42 hours of A-array VLA data at 1.4 GHz have been combined to image a 10-arcmin field centred on the Hubble Deep Field (HDF). This area also includes the Hubble Flanking Fields (HFF). A complete sample of 92 radio sources with  $S_{1.4} > 40 \mu\text{Jy}$  was detected using the VLA data alone and then imaged with the MERLIN+VLA combination. The combined images offer: i) higher angular resolution (synthesised beams of diameter 0.2–0.5 arcsec); ii) improved astrometric accuracy and iii) improved sensitivity compared with VLA-only data. The images are amongst the most sensitive yet made at 1.4 GHz, with rms noise levels of  $3.3 \mu\text{Jy beam}^{-1}$  in the 0.2-arcsec images. Virtually all the sources are resolved, with angular sizes in the range 0.2 to 3 arcsec. The central 3-arcmin square was imaged separately to search for sources down to  $27 \mu\text{Jy}$ . No additional sources were detected, indicating that sources fainter than  $40 \mu\text{Jy}$  are heavily resolved with MERLIN and must have typical angular sizes  $>0.5$  arcsec. Radio sources associated with compact galaxies have been used to align the HDF, the HFF and a larger CFHT optical field, to the radio-based International Celestial Reference Frame. The *HST* optical fields have been registered to  $< 50$  mas in the HDF itself, and to  $\leq 150$  mas in the outer parts of the HFF. We find a *statistical* association of very faint ( $\geq 2 \mu\text{Jy}$ ) radio sources with optically bright HDF galaxies down to  $\sim 23$  mag. Of the 92 radio sources above  $40 \mu\text{Jy}$ ,  $\sim 85$  per cent are identified with galaxies brighter than  $I = 25$  mag; the remaining 15 per cent are associated with optically faint systems close to or beyond the HFF (or even the HDF) limit. The high astrometric accuracy and the ability of radio waves to penetrate obscuring dust has led to the correct identification of several very red, optically faint systems including the the strongest sub-mm source in the HDF, HDF850.1. On the basis of their radio structures and spectra 72 per cent (66 sources) can be classified as starburst or AGN-type systems; the remainder are unclassified. The proportion of starburst systems increases with decreasing flux density; below  $100 \mu\text{Jy}$   $>70$  per cent of the sources are starburst-type systems associated with major disc galaxies in the redshift range 0.3 – 1.3. *Chandra* detections are associated with 55 of the 92 radio sources but their X-ray flux densities do not appear to be correlated with the radio flux densities or morphologies. The most recent sub-mm results on the HDF and HFF do not provide any unambiguous identifications with these latest radio data, except for HDF850.1, but suggest at least three strong candidates.

**Key words:** galaxies: evolution – galaxies: active – galaxies: starburst – cosmology: observations – radio continuum: galaxies

## 1 INTRODUCTION

Radio observations allow us to probe the nuclear regions of galaxies which are obscured by gas and dust in other wavebands. In addition, radio observations with high angular resolution can distinguish, on morphological grounds, between emission that is driven by star-formation and that which is driven by Active Galactic Nuclei (AGN). While sub-mm wavelengths provide one means of detecting star-formation in the early Universe, through redshifted infrared radiation from dusty star-forming regions, current sub-mm instruments do not have sufficient angular resolution to avoid source blending in deep sub-mm fields, or the astrometric capability to avoid confusion in crowded optical/NIR fields. Sensitive, high angular-resolution radio observations are currently the best way to uniquely identify the optical counterparts to this population. Furthermore, because of the negative  $K$ -correction, dusty galaxies observed at sub-mm wavelengths preferentially lie at high redshifts whereas radio observations are sensitive to a wide range of redshifts and to a mix of starburst and AGN activity and hence provide complementary information on the population of distant galaxies.

The *Hubble Space Telescope* (*HST*) has been used to image a window on the distant universe to very high sensitivity. The central Hubble Deep Field (HDF) and surrounding Hubble Flanking Fields (HFF) are complete to  $R$  magnitudes of 29 and 25 respectively (Williams et al. 1996). The HDF region was selected to avoid known bright galaxies in any observable waveband.

We report here the results from our high-resolution, high-sensitivity 1.4-GHz MERLIN+VLA study of the  $\mu\text{Jy}$  sources found in a 10-arcmin field enclosing both the HDF and HFF, together with a more sensitive search for radio sources in a 3-arcmin square field enclosing the HDF itself. These represent amongst the most sensitive 1.4-GHz observations yet made and together with their high angular resolution (0.2 arcsec) and astrometric positional accuracy (tens of mas) these data allow, for the first time, detailed imaging and accurate identification of  $\mu\text{Jy}$  radio sources.

This work represents a major extension to the original 1.4-GHz VLA results reported in Richards et al. (1999) and Richards (2000) providing better astrometry, more sensitive maps, and higher angular resolution. It also complements and adds to the work at 8.4 GHz reported by Fomalont et al. (2002) and Richards et al. (1998).

In Sections 2 and 3, we summarize the VLA and MERLIN observations and the procedures adopted to make the radio images. In Section 4 we describe in some detail the process of alignment of the optical and radio fields in order to achieve a registration accuracy of  $<50$  mas (HDF) to  $<150$  mas (HFF/outer 10-arcmin field). In Section 5 we discuss the individual radio/optical objects in the 10-arcmin field. In Section 6 we outline the different procedure adopted to image the 3-arcmin field and discuss the statistical association of very weak radio sources with optical objects down to  $R = 25$  mag. In Section 7 we discuss the structural properties of the  $\mu\text{Jy}$  radio sources, their optical identifications and redshifts, their luminosities and inferred star-formation rates. In Section 8 we make comparisons with other observations in radio, sub-mm, infra-red, and X-ray wavebands; whilst in Section 9 we discuss the optically faint systems.

We look forward to the possibilities opened up by the next generation of telescopes in Section 10 and our overall conclusions from this deep radio study are presented in Section 11.

## 2 THE RADIO OBSERVATIONS AND DATA REDUCTION

### 2.1 The VLA observations

The detailed description of the VLA observations and calibration are given in Richards (2000) and we merely summarize the work here for completeness. We observed an area centred on the Hubble Deep Field and located at R.A.  $12^{\text{h}} 36^{\text{m}} 49^{\text{s}}.4$  Dec.  $+62^{\circ} 12' 58''.00$  (J2000) with the VLA in A-array for a total of 50 hours at 1.4 GHz. In order to minimise chromatic aberration, we observed in ‘pseudo-continuum mode’ with  $7 \times 3.125$  MHz channels centred on intermediate frequencies 1365 MHz and 1435 MHz, frequency windows previously established to be relatively free of radio frequency interference.

After time-averaging the data to 13 seconds and significant tapering in the spatial frequency plane, preliminary 10-arcsec resolution maps were made covering the field out to the first side-lobe of the primary beam – about  $0^{\circ}.8$  from the field centre. These were then searched for bright, confusing sources with flux densities whose side-lobes might contaminate the noise characteristics of the inner portion of the field.

Each confusing source above 0.5 mJy was imaged and heavily CLEANed using the full resolution data set. Because of changes in the primary beam response across our 44-MHz bandpass it was necessary to deconvolve each of the confusing sources in spectral-line mode separately from each frequency channel. Furthermore, the confusing sources were independently deconvolved for each hand of circular polarization; this was to account for the beam-squint of the VLA antennas which produces small but significant differences for each hand of polarization for sources on the edge of the primary beam. The CLEAN components were then Fourier transformed and subtracted from the visibility data which were then used to image the inner few arcmin of the field. Following this procedure, the rms noise was found to be about 50 per cent higher than expected from receiver noise alone. In particular, a few side-lobes from particularly strong confusing sources ( $S > 10$  mJy) located near the half-power point of the primary beam were still apparent.

By examining the images made from 30 minute segments of data, we isolated a few time intervals where the visibility data appeared to be corrupted, possibly due to incomplete confusing source subtraction associated with telescope pointing errors, or perhaps low level interference. We deleted all data segments where the rms noise exceeded the mean value by greater than 50 per cent. This amounted to about 7 hours of data and, in all, about 42 hours of high quality data were used to construct the final images. In the final VLA images we achieved an rms noise of  $7.5 \mu\text{Jy beam}^{-1}$ , compared with a theoretical value closer to  $5 \mu\text{Jy beam}^{-1}$ . 92 sources with flux densities  $>40 \mu\text{Jy}$  ( $5.3\sigma$ ) were reliably detected in the 10-arcmin  $\times$  10-arcmin field.

## 2.2 The MERLIN observations

We observed the same position with the Multi-Element Radio Linked Interferometer Network (MERLIN) at 1.4 GHz in February 1996 and April 1997 for a total of 18.23 days. These observations included the 76-metre diameter Lovell Telescope which increases the array sensitivity by a factor  $\sim 2.4$  compared with identical observations excluding the Lovell Telescope. Observations with a single intermediate frequency, were centred on 1420.0 MHz with  $32 \times 0.5$ -MHz channels to allow imaging over a wide field 10 arcmin on a side (comparable with the primary beam of the Lovell Telescope HPBW=12.4 arcmin). Data from the correlator were recorded every 4 seconds. As with the VLA data, correlator limitations resulted in only parallel hands of circular polarization being correlated, thus no linear polarization information is available.

The interferometric phases were calibrated by observing the nearby 0.4 Jy phase calibration source J124129+622041 with a duty cycle of 8:2 minutes (source:calibrator). The visibility amplitudes were calibrated against 3C286 and B1803+784 with assumed flux densities of 14.774 Jy and 1.914 Jy respectively (Baars et al. 1977). Bandpass calibration was performed using B1803+784. Visibilities corrupted by instrumental phase errors, telescope errors, or external interference were flagged and discarded. Finally, the visibilities were re-weighted to reflect the differing sensitivities of the various telescopes involved in the MERLIN array. Due to the high angular resolution of MERLIN, its lack of short interferometer spacings, and the effect of the primary beam of the Lovell Telescope, no significant problems with confusing sources outside the 10-arcmin field were encountered. However, the four strongest sources within the 10-arcmin field were mapped and their CLEAN components subtracted from the MERLIN data, prior to the MERLIN+VLA imaging of the remaining 88 weaker sources detected by the VLA. In addition, the ‘subtracted data’ set was used for the imaging of the 3-arcmin field. The frequency channels at the extreme ends of the passband are subject to a loss of sensitivity due to bandwidth limitations on the microwave radio links. The lowest rms noise value was found when excluding the lowest three and the highest channel, resulting in a final bandwidth of 14 MHz. The rms noise achieved in naturally-weighted images from the MERLIN data alone was  $5.9 \mu\text{Jy beam}^{-1}$  which is within 10 per cent of the theoretical value.

## 3 THE RADIO IMAGES

### 3.1 Data and image combination

Since the correlators used for the observations of the HDF and HFF were optimally configured for the two separate arrays, the MERLIN and VLA visibility datasets are fundamentally different in structure, containing differing numbers of intermediate frequencies, frequency channels, and channel bandwidths. For this reason, combining the visibility datasets in the AIPS software package proved wholly impracticable, not least due to the size of the visibility datasets which, in combination, proved far too large for the software package as implemented to handle. The data were therefore combined in the sky-plane rather than the  $uv$  plane.

For all the 92 radio sources detected by the VLA in the

10-arcmin field, individual ‘postage-stamp’ maps were made centred on each source from both the VLA and MERLIN datasets separately. No deconvolution was performed prior to any image combination; thus the ‘dirty maps’ and ‘dirty beams’ were made from each naturally-weighted dataset separately. In order to retain optimum Fourier Transform gridding for each dataset, a different cell-size was selected for each array (MERLIN 0.05 arcsec, VLA 0.4 arcsec). The VLA ‘dirty maps’ and ‘beams’ were then re-gridded to the cell-size of the MERLIN images and then averaged with them to produce combination ‘dirty maps’ and a combination ‘dirty beam’. We gave equal statistical weight to each input image since the MERLIN and VLA images were of comparable sensitivity. This process is equivalent to combining the data sets prior to Fourier transformation into the sky plane. The central quarters of these combination images were then deconvolved with a conventional CLEAN algorithm (Högbom, 1974) resulting in deconvolved images 25.6 arcsec on a side.

To demonstrate the equivalence of sky plane and visibility plane combination, we have performed a test with one  $307\text{-}\mu\text{Jy}$  source, J123649+620738, which lies 320 arcsec almost due south from the field centre, just outside the 10-arcmin field. The MERLIN and VLA datasets were separately phase rotated to the position of this test source and then averaged in time and to a single frequency channel. Averaging restricts the field of view to a small region around the test source, but simplifies and compresses the datasets by a considerable amount allowing data combination prior to Fourier transformation. From the averaged datasets, a ‘dirty map’ and ‘dirty beam’ were then made and the map cleaned using the sky-plane combination method described above. Separately, the averaged data were then combined in the visibility plane and a second ‘dirty map’ and ‘dirty beam’ were then made and CLEANed. The two CLEANed images are shown in Fig. 1; two compact components are embedded within a region of emission extending over  $\sim 1.5$  arcsec. The two images are essentially identical; the difference between them is noise-like with a peak difference of under  $4 \mu\text{Jy beam}^{-1}$  in the contoured area.

We also constructed a mini-mosaic of the inner 3 arcmin  $\times$  3 arcmin field (see Section 6) using the sky-plane combination technique in order to search for additional sources below the VLA-alone  $40\text{-}\mu\text{Jy}$  detection threshold. In this case, however, 72 contiguous images were made in an  $8 \times 9$  grid centred on the HDF, using a pixel size of 0.0625 arcsec. We spaced the grid so that the central 410 – 412 pixels (within a CLEANed area of  $512 \times 512$  pixels) of the images abutted one against another so as to cover the field completely allowing for sky curvature. We stress that these images are not centred on existing VLA-only detections as is the case with the images derived for the 10-arcmin field. The image coverage of the 3- and 10-arcmin fields is illustrated in Fig. 2.

Primary beam corrections for combination images within the the 10-arcminute field are small since they are dominated by the 25-m antennas of the VLA and MERLIN which have a half-power beam width (HPBW) of  $\sim 35$  arcmin at 1.4 GHz. The Lovell telescope has an HPBW of 12 arcmin but on a baseline to a 25-m antenna the combined HPBW is  $\sim 20$  arcmin (see Strom (2004) for the derivation). With respect to a source at the field centre, the flux of a source 5 arcmin distant is only depressed by 1 per cent and 12 per cent for 25-m–25-m and 25-m–Lovell

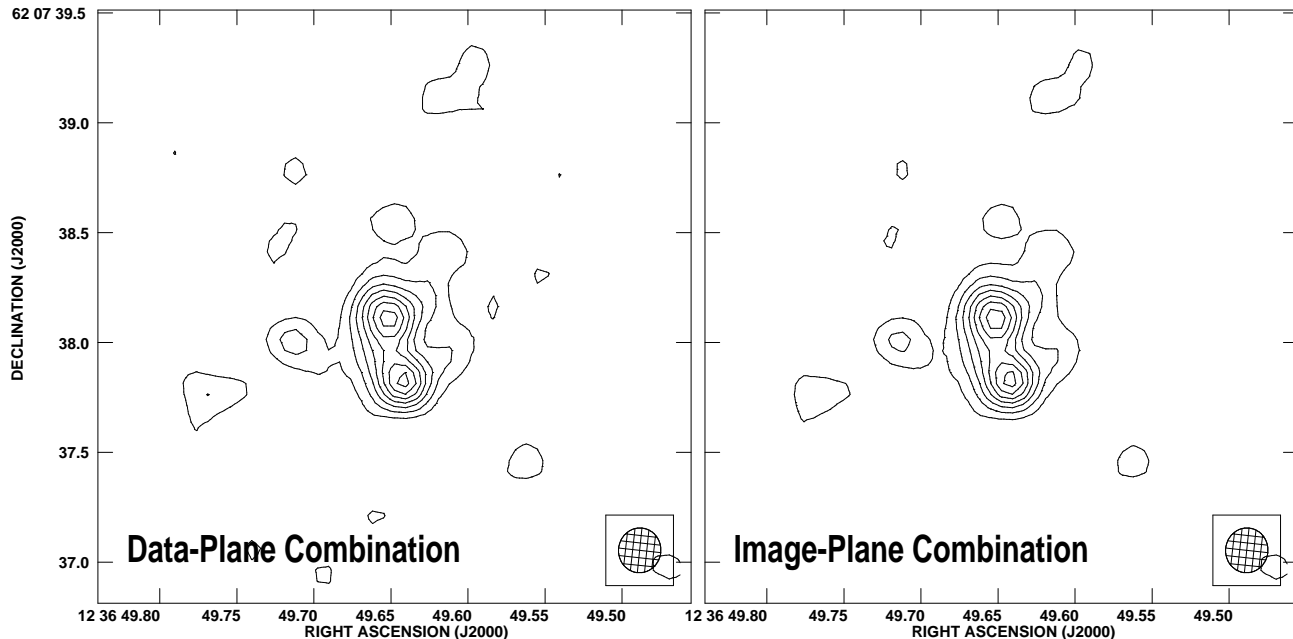


**Figure 1.** A comparison of CLEANed images using MERLIN+VLA combination in the visibility (left) and image (right) planes. The contour interval is linear with a lowest contour value of  $10 \mu\text{Jy beam}^{-1}$ .

baselines respectively. We compared the images from VLA-only and MERLIN+VLA combinations and estimated that, in the combination images, the measured fluxes 5 arcmin from the field centre are depressed by only  $\sim 6$  per cent and for the majority of sources in the 10-arcmin field the effect is significantly less. The position uncertainties given in Table A1 take into account the local increase in noise due to the various aberrations and the quoted flux densities listed in Table A2 have been corrected for primary beam effects. No correction has been made to the contoured combination images shown in Appendix B.

### 3.2 Positional comparisons with previously published 1.4 GHz images

Within each of the ‘postage-stamp’ images, the sky is treated as flat. However, the image offset from the interferometer pointing centre is corrected for sky curvature so as to avoid image distortion at large offsets. Richards (2000) imaged the entire 40-arcmin VLA primary beam using 16 facets of size  $14 \text{ arcmin} \times 14 \text{ arcmin}$ . There is measurable sky distortion near the edges of these facets which introduce positional offsets of up to 0.2 arcsec for individual sources. However, after correction for these known effects, we find that the MERLIN and VLA positions agree to within 15 mas. The MERLIN+VLA combination images are of significantly greater angular resolution than the VLA-only images of Richards (2000). Furthermore, at MERLIN resolutions the vast majority of these weak radio sources are resolved. The positions quoted in Table A1 are for the brightest features in the combination images, and for the reasons just given, differ from those quoted in Richards (2000). A full analysis of the astrometric alignment of this multiple small-image technique is given in Section 4.1 where we find that the quoted positions

for the MERLIN+VLA combination images in Table A1 lie on the International Celestial Reference Frame (ICRF) to within 15 mas.

## 4 THE OPTICAL IDENTIFICATIONS OF THE RADIO SOURCES

Williams et al. (1996) describe the WFPC2 observations and data reduction procedure and present a complete catalogue of objects detected within the HDF. In the  $4.7 \text{ arcmin}^2$  region of the HDF, objects as faint as  $U = 27.6$ ,  $B = 28.1$ ,  $V = 28.7$ , and  $I = 28.0$  (AB magnitudes) are detected at the  $10 \sigma$  level. In addition to the HDF, eight *HST* exposures of one orbit were taken in *I*-band (F814) in flanking fields (HFF) immediately adjacent to the HDF (Williams et al. 1996). The point source sensitivity for each of these frames is about  $R = 25 \text{ mag}$ .

In the process of aligning the optical and radio fields, we also used a deep CFHT *I*-band frame taken by Barger et al. (1999). This field is 9 arcmin on a side and encloses both the HDF and HFF frames. The CFHT field also enabled additional optical identifications outside the HDF and HFF to be made. This field has a resolution of about 1.5 arcsec and its limiting magnitude is  $R \sim 26$ .

### 4.1 Radio/optical astrometric alignment

In order to make reliable optical identifications of the radio sources, it is important to align the *HST* images with the radio images which are closely tied to the ICRF (see below). Although the fine guidance system of the *HST* is accurate to a few mas, intrinsic uncertainties in the *HST* Guide Star Catalog positions on the order of 1–2 arcsec are the limiting

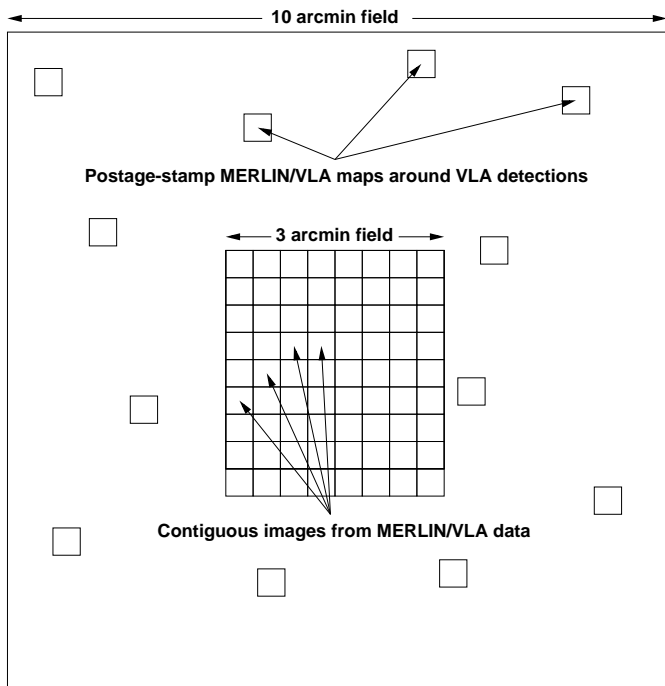


**Figure 2.** Schematic of the image coverage in the 3- and 10-arcmin fields. Only a few of the 92 ‘postage-stamp’ images are indicated for simplicity.

source of error in tying the *HST* astrometric grid to the ICRF.

#### 4.1.1 Radio astrometry

The position grid of the VLA HDF radio images is tied to the radio source J121711+583526 with an assumed position of R.A.  $12^{\text{h}} 17^{\text{m}} 11^{\text{s}}.0202$  and Dec.  $+58^{\circ} 35' 26''.228$  (J2000) (Patnaik et al. 1992). This source has quoted positional errors of 13 mas with respect to the ICRF. Subsequently, the position of the compact core of this source has been established at higher radio frequencies to an accuracy of order 1 mas with respect to the ICRF (Beasley et al. 2001). However, the object shows significant jet emission, especially at 1.4 GHz, and positional blending between core and jet components result in an overall radio positional uncertainty of  $\sim 10$  mas. The accuracy of transferring the position of J121711+58585 to the position of the VLA HDF images is much better than 50 mas, derived from an estimate of typical long-term systematic phase errors and the angular separation in the sky between J121711+58585 and the Hubble fields.

The position of the compact MERLIN phase calibration source, which lies less than 40 arcmin from the HDF field centre (J124129+622041, R. A.  $12^{\text{h}} 41^{\text{m}} 29^{\text{s}}.589115$  Dec.  $+60^{\circ} 20' 41''.32402$  (J2000), has been established to lie on the ICRF to better than 1 mas (Beasley et al 2001). The error in transferring the position of J124129+622041 to the position of the MERLIN images is less than 5 mas, again

derived from typical systematic phase performance and the calibration source to HDF separation.

As an internal consistency test, we compared the independently derived MERLIN and VLA radio positions for the compact flat-spectrum AGN source J123714+620823 (which lies some 5 arcmin from the HDF field centre towards the edge of the 10-arcmin field); they agree to better than 12 and 10 mas in Right Ascension and Declination respectively. This is consistent with the quoted phase calibrator position errors in Patnaik et al. (1992). We are therefore confident that the radio positions for the MERLIN+VLA combination images presented in this paper lie on the ICRF to within 15 mas.

#### 4.1.2 Optical – radio alignment of the CFHT field

Each *HST* WFPC2 frame typically contains too few radio detections to align the radio and optical images directly. An intermediate stage is thus required. We have therefore aligned the ground-based CFHT deep *I*-band image covering a 9-arcmin field centred on the HDF (Barger et al. 1999) under the radio detections. The CFHT image has, to first order, already been corrected for geometrical distortion. However, a further correction was made in order to optimise the alignment of this frame with respect to the radio source positions and hence the ICRF. This was achieved by fitting the positions of 36 galaxies identified with brighter radio sources in the 10-arcmin radio field. Both 4- and 6-parameter fits were performed. The 4-parameter solution fits for an  $x$  and  $y$  shift, a rotation, and a stretch term. The 6-parameter fit allows for non-perpendicular  $x$ - $y$  axes with a further stretch term. The 6-parameter solution was found to be no better than the 4 parameter solution since the two axes were found to be perpendicular to better than 0.01 degrees. We adopted the 4-parameter solution and applied these to positions derived from the CFHT frame.

The fitting residuals in the outer parts of the CFHT frame (typically outside the area of both the HDF and HFF) show that there are small but significant departures from the model. The fitting residuals are shown in Fig. 3. Where it was felt that the residuals showed a consistent offset over a region in the outer parts of the CFHT frame, a further empirical positional shift correction was made. These final corrections are also marked in Fig. 3.

#### 4.1.3 Alignment of CFHT and HDF/HFF WFPC2 frames

After applying positional shifts from the 4 parameter solution (derived from the whole of the CFHT frame), the rms of the fitted residuals in the central part of the image, which overlies the 3 HDF frames, was found to be 66 mas. For this sub-region only, a small modification was made to the CFHT shift parameters in order to optimise the optical to radio alignment within the HDF itself resulting in a reduction of the rms fitted residuals to 41 mas. The rms of the fitted residuals for the inner flanking fields (within 2.5 arcmin of the HDF pointing centre) was found to be 118 mas. For the outer flanking fields the rms of the residuals was found to be 143 mas.

Optically compact galaxies in each WFPC2 frame were then registered over the same galaxy in the positionally corrected CFHT image. By this means, the WFPC2 frames

**Table 1.** Astrometric alignment errors in the 10-arcmin field.

Registration Error	Sub-Region of the 10-Arcmin Field			
	HDF	Inner HFF	Outer HFF	Beyond HFF
Radio $\Leftrightarrow$ ICRF (MERLIN $\Leftrightarrow$ VLA $\Leftrightarrow$ ICRF)	<15mas	<15mas	<15mas	<15mas
Optical $\Leftrightarrow$ ICRF (MERLIN+VLA $\Leftrightarrow$ CFHT $\Leftrightarrow$ <i>HST</i> )	<50mas	50-100mas	100-150mas	150-250mas

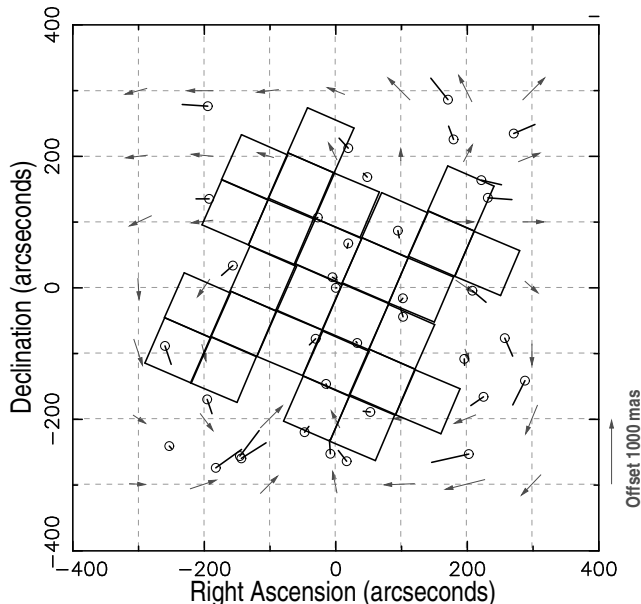


**Figure 3.** Fitting residuals for the CFHT frame (Barger et al. 1999); the HDF and HFF WFPC2 frames are shown as solid lines. Circles and bars mark the residual offsets from the 4-parameter fitted solution for a number of radio sources with compact nuclear components associated with compact optical galaxies. Arrows at grid intersections mark the derived distortion terms used to correct galaxy positions in the outer part of the CFHT frame after applying the 4-parameter solutions. A 1000 mas scale for the bars and arrows is shown at bottom right.

were aligned with the radio frame and therefore the ICRF. The optical to radio registration errors are still the dominant source of errors in this procedure. Within the HDF itself, the residual optical registration error is less than 50 mas, rising to approximately 120 mas in the inner parts of the HFF, and to approximately 150 mas at the edge of the HFF. At the edge of the CFHT frame the registration error is  $\sim$ 250 mas. These astrometric errors are summarised in Table 1.

## 5 THE 10-ARCMINUTE FIELD

In this section we present and discuss the detailed radio structures found for the complete sample of 92 weak radio

sources stronger than  $40 \mu\text{Jy}$  ( $5.3\sigma$ ) detected in the VLA-only dataset and lying within the 10-arcmin field centred on the HDF. To repeat, for each source combination MERLIN+VLA ‘postage-stamp’ images were made with a deconvolved area  $25.6 \times 25.6 \text{ arcsec}^2$  around the VLA position. Three sizes of restoring beam were employed: the formal fitted beam of  $0.204 \times 0.193 \text{ arcsec}^2$  with major axis position angle  $-6^\circ$ , and larger circular beams of 0.3 arcsec, and 0.5 arcsec. The complete list of source details is given in Tables A1 and A2, and the radio structures at the angular resolution shown in column 5 of Table A1 are displayed in Fig. C1, overlaid on the astrometrically-aligned optical images. The optical images are either WFPC2 HDF/HFF frames or, for those regions outside the HFF, the CFHT frame. The additional source information found in the central 3-arcmin field is presented in Table 2 and discussed in Section 6. The high resolution of the HDF/HFF observations allows us to concentrate on characterising the phenomena responsible for radio emission; these may coexist with other processes in the same host galaxy.

### 5.1 Classifying the radio structures

Although few of these  $\mu\text{Jy}$  radio sources are appreciably resolved by the 2-arcsec beam of the VLA A-array image, virtually all are resolved by the MERLIN+VLA combination showing that they have angular sizes in the range 0.2 to 3 arcsec, typically smaller than the sizes of the optical galaxy images. Fig. 4 shows the observed distribution of angular sizes. The structural description scheme adopted in Table A2 is as follows:

- FRI** : Fanaroff & Riley (1974) Type I ‘classical’ double structure.
- WAT** : Wide-Angled-Tail ‘classical’ double structure.
- C** : Compact component at 0.2-arcsec resolution.
- C1E** : Compact component + one-sided extended emission.
- CE** : Compact component + two-sided extended emission.
- E** : Extended emission with no compact component. Note that most of the E sources have sub-galactic dimensions.
- +** : Low surface-brightness emission lies beyond that re-

**Table 2.** 1.4-GHz radio sources detected at  $\geq 7\sigma$  with 0.5-arcsec resolution in the 3-arcmin field. All sources were also detected by the VLA alone at 1.4 GHz (see Tables A1 and A2).

Name	$P_{1.4}$ ( $\mu\text{Jy beam}^{-1}$ )	$S_{1.4}$ ( $\mu\text{Jy}$ )	Size "×"	P.A. °	Position (P) (J2000)	Other Information
J123636+621320	29	50	(0.66×0.46)±0.13	75±30	12 36 36.8982 +62 13 20.320	
J123642+621331	348	472	(0.339×0.266)±0.001	103±1	12 36 42.0959 +62 13 31.410	V <sub>8.4</sub> I
J123644+621133	621	791	(0.317×0.166)±0.001	6±1	12 36 44.3894 +62 11 33.110	V <sub>8.4</sub> H
J123646+621448	79	101	(0.425×0.255)±0.001	159±1	12 36 46.0607 +62 14 48.728	V <sub>8.4</sub>
J123646+621404	142	199	< 0.42×< 0.42 —	— —	12 36 46.3352 +62 14 04.694	V <sub>8.4</sub> HI
J123649+621313	31	134	(1.46×0.65)±0.16	80±6	12 36 49.6830 +62 13 12.885	V <sub>8.4</sub> HI
J123651+621221	56	130	(0.84×0.40)±0.07	88±5	12 36 51.7238 +62 12 21.408	V <sub>8.4</sub> HI
J123652+621444	106	122	(0.29×0.19)±0.06	110±20	12 36 52.8865 +62 14 44.067	V <sub>8.4</sub> H
J123653+621139	41	53	(0.43×0.23)±0.16	112±19	12 36 53.3754 +62 11 39.614	V <sub>8.4</sub> I
J123656+621207	27	30	< 0.64×< 0.64 —	— —	12 36 56.5570 +62 12 07.446	H
J123701+621146	29	130	(1.36×0.60)±0.18	6±7	12 37 01.5745 +62 11 46.738	V <sub>8.4</sub> I

V<sub>8.4</sub> – also detected by the VLA alone at 8.4 GHz

H – radio source located in the Hubble Deep Field

I – radio contours overlap the  $3\sigma$  position box of an *ISO* detection

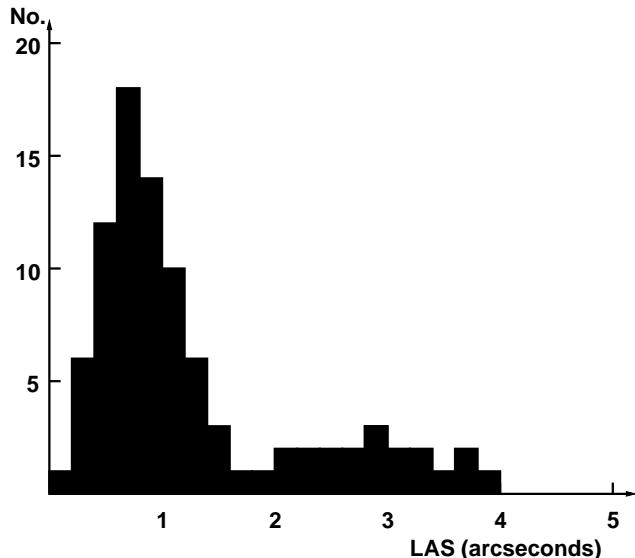


**Figure 4.** Distribution of largest angular sizes for 91 of the 92 radio sources studied in the 10-arcmin field and listed in Table A2. The remaining source, J123644+621133, has a largest angular size of 12 arcsec.

gion shown in the MERLIN/VLA image (detected by the VLA alone).

There are very few radio structures typical of high luminosity sources (i.e. twin lobes on either side of the parent galaxy) and those that are found are associated with the relatively stronger, mJy, sources. The vast majority of  $\mu\text{Jy}$  sources in the 10-arcmin field have radio structures with sub-galactic sizes.

We have compared our 1.4-GHz flux densities with those measured by the VLA at 8.4 GHz (Richards et al. 1998) to derive radio spectral indices for our sample (see column 5 in Table A2 and table 5 in Richards 2000).

The classification scheme adopted for the radio sources is as follows:

**AGN/AGN Candidate:** We classify a source as an ‘AGN’ if it has a flat or inverted radio spectrum accompanied by a compact core and one or two-sided extended structure<sup>1</sup>. Sources with only some of these characteristics are classified as ‘AGN candidates’.

**Starburst/Starburst Candidate:** We classify a source as a ‘Starburst’ if it has a steep radio spectrum, is extended on sub-galactic scales (often aligned with the galaxy major axis) and is also detected by the Infrared Space Observatory (*ISO*) (Goldschmidt et al. 1997; Aussel et al. 1999). The correlation between radio and IR luminosity is so close (Carilli & Yun 1999; Garrett 2002) that an *ISO* detection, especially at 15  $\mu\text{m}$ , is a strongly statistically significant indicator that at least the proportional fraction of the radio emission is also of starburst origin. Sources with only some of these characteristics are classified as ‘Starburst Candidates’. Three high-redshift ( $z > 2$ ) starburst systems which show evidence for an additional embedded AGN component, such as a compact core or hard X-ray emission (see Table A2), are designated as S\*. Alexander et al. (2002) discuss the likelihood of 15- $\mu\text{m}$  sources with hard X-ray emission harbouring AGN.

**Unclassified:** Sources with complex radio structures which could be associated with either AGN or starburst activity are listed as ‘unclassified’, for example if the radio emission is more extended than optical emission and there is a dearth of other evidence.

Appendix B gives a source-by-source summary of detections in the 10-arcmin field.

<sup>1</sup> J123725+621128 has a steep spectrum at VLA resolution but the MERLIN+VLA images show that it is unmistakably an AGN with large radio lobes

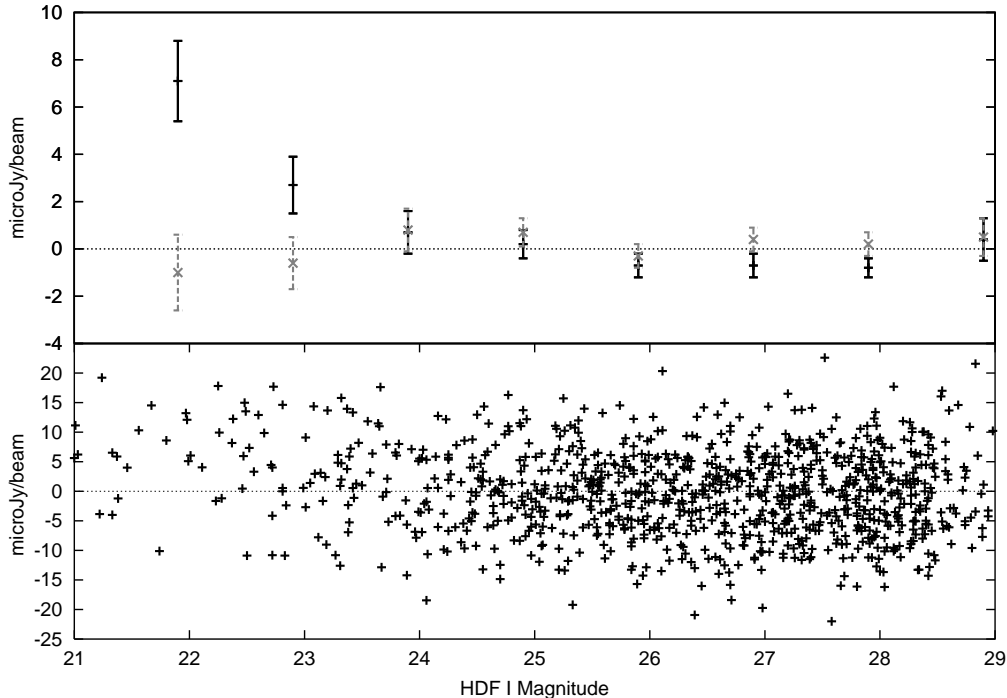


**Figure 5.** (Upper) radio brightness at 1.4 GHz smoothed to 1-arcsec resolution at the position of known galaxies, plotted as black + signs against the WFPC2 galaxy *I* magnitude, in 1-magnitude bins. The control data are displayed as grey × signs and incorporate a random 7-arcsec shift applied to the radio positions in both R.A. and Dec.. (Lower) data for the known galaxies shown unsmoothed.

## 6 THE THREE-ARCMINUTE FIELD

### 6.1 Mapping and analysis

The innermost  $3.41 \times 3.84$  arcmin<sup>2</sup> of the radio field was examined in more detail, and is referred to as the ‘3-arcmin field’. A grid of  $8 \times 9$  maps was made from the calibrated MERLIN and VLA data sets as described in Section 3.1. We also restored the CLEAN components for the four bright sources in this region which had already been subtracted as described in Section 2.2.

The noise fluctuations at low brightness levels are higher than expected for a pure Gaussian distribution. A number of factors are likely to contribute to this excess, as discussed in Section 2.1. These include pointing fluctuations, residual ripples due to sources in the outer parts of the primary beam and residual side-lobes of the brighter sources in the field. Since such effects are likely to produce as many negative deviations as positive, we have adopted a pragmatic approach to establishing real source thresholds.

Initially each of the 72 maps was examined for regions with brightness above  $25 \mu\text{Jy beam}^{-1}$ ; 42 of them had no such peaks. The brightness distribution in these ‘source-free’ maps was statistically analysed. The rms noise level with a 0.5-arcsec restoring beam is  $3.9 \mu\text{Jy beam}^{-1}$  with no positive or negative peaks above  $\pm 7\sigma_{\text{rms}}$ . The noise level with the smallest 0.2-arcsec restoring beam is  $3.3 \mu\text{Jy beam}^{-1}$  with no peaks above  $\pm 8\sigma_{\text{rms}}$ . In the other 30 images, positive regions above these levels ( $27$  and  $25 \mu\text{Jy beam}^{-1}$  at 0.5- and 0.2-arcsec resolutions respectively) are therefore considered reliable detections.

Eleven positions have peaks above  $27 \mu\text{Jy beam}^{-1}$  (see Table 2). All these sources coincide with VLA 1.4-GHz

detections with flux densities  $> 40 \mu\text{Jy}$  (total); they can all be regarded as secure and thus the sample is complete to this limit. The positions and sizes of these eleven sources were found by fitting Gaussian components in the image plane. Nine sources are significantly resolved, and one (J123656+621207) is too weak for its size to be measured reliably. One object in Table A1 (J123646+621445), which also lies in the 3-arcmin field, is so spatially resolved as to fall below the  $27 \mu\text{Jy beam}^{-1}$  detection threshold and thus does not appear in Table 2. This imaging exercise therefore revealed no new sources in the 3-arcmin field in the brightness range  $27$ – $40 \mu\text{Jy beam}^{-1}$ . Note however that at the same time as reducing the detection threshold from  $40$  (VLA-only) to  $27 \mu\text{Jy beam}^{-1}$ , we also increased the angular resolution from 2 arcsec (VLA-only) to 0.5 arcsec. The slope of the integral source counts around  $40 \mu\text{Jy}$  is  $-1.4$  (Richards 2000) and one would therefore expect to find  $\sim 8$  additional sources within the 3-arcmin field in the flux density range  $27$ – $40 \mu\text{Jy}$ , including one compact AGN. Since we do not detect any new sources, we infer that most objects weaker than  $40 \mu\text{Jy}$  are heavily resolved with a 0.5-arcsec beam, do not contain compact radio components  $> 27 \mu\text{Jy}$  and must have angular sizes  $> 1$  arcsec. We ascribe the failure to detect an additional compact AGN source to chance. The planned extension of the investigation to the complete mapping of the 10-arcmin field (see Section 10) will provide additional constraints on this interpretation.

### 6.2 Statistical comparison with HDF galaxies

For the part of the 3-arcmin field which overlies the central HDF area itself, the MERLIN+VLA images were smoothed



to 1-arcsec resolution, after excluding all 11 significant individual source detections (points above  $+27 \mu\text{Jy beam}^{-1}$ ). The radio brightness was then measured at the positions of all catalogued HDF galaxies (Williams et al. 1996). The results are shown in Fig. 5, binned by  $I$ -band magnitude. The figure shows that sources over an order of magnitude weaker than our detection threshold ( $40 \mu\text{Jy}$ ), are statistically associated with galaxies brighter than  $I \sim 23$  mag. A control sample which incorporates a random 7-arcsec shift applied to the radio measurement positions, in both R.A. and Dec. with respect to the optical galaxies shows no excess of detected brightness. Thus the source population down to a few  $\mu\text{Jy}$  shares similar properties with the 10-arcmin field sample, being identified statistically with the brighter HDF galaxies.

## 7 PROPERTIES OF THE RADIO SOURCES

### 7.1 Source sizes

As summarised in Fig. 4, the great majority of the  $\mu\text{Jy}$  source population have radio angular sizes in the range 0.2 arcsec to 3 arcsec. Only one source in the sample of 92 objects is unresolved (J123714+620823). Only two sources (J123644+621133 and J123725+621128) show classical radio structures usually associated with high luminosity AGN, and both of these are representative of the tail of the mJy source population rather than that of the  $\mu\text{Jy}$  sources. One other AGN system, (J123652+621444), shows evidence from WSRT observations of a possible one-sided low surface-brightness jet structure extending for some 30 arcsec with an implied size of around 100 kpc.

Notwithstanding that perhaps a total of 10 per cent of low-surface brightness extended sources have been missed by the original VLA-only survey (see Section 8.1), the great majority of objects in the 10-arcmin field have radio structures extended predominantly on galactic and sub-galactic scales. Their radio structures have been defined and discussed in Section 5.1 and Appendix B respectively. The typical source angular scale appears similar down to  $27 \mu\text{Jy}$  and even beyond (see Section 6).

The fact that the typical angular size of  $\mu\text{Jy}$  sources is  $\sim 1$  arcsec may have implications for future deep surveys with the Square Kilometre Array (SKA) which could encounter a natural confusion limit. If the slope of the source counts at 1.4 GHz remains as steep as  $-1.4$  then surveys, with limiting flux densities 100 times fainter than the present one, will reach surface densities  $>500$  sources  $\text{arcmin}^{-2}$  (similar to the surface density of optical galaxies in the HDF). If the typical source size remains  $\sim 1$  arcsec then the proportion of sky covered with radio sources,  $C$ , will be  $>0.14$ . If  $C > 0.05$  significant blending of sources begins to occur (Fomalont et al. 2002) and obviously if  $C > 0.14$  a large amount of source blending would result, regardless of the size of the synthesized observing beam. This simple inference depends, however, on two large extrapolations (source counts and sizes). The optical HDF is not significantly confused and it could be, for example, that the fainter radio sources are smaller, being associated with the fainter, smaller, irregular galaxies; this could reduce  $C$  to below the natural confusion limit.

### 7.2 Optical identifications and redshifts

Sixty-one of the 92 sources (65 per cent) in the 10-arcmin field have measured spectroscopic or estimated photometric redshifts (at the time of performing this analysis). Fig. 6 shows the redshift distribution for each of the three classifications. Note that the highest redshift source, J123642+621331, appears to contain a compact AGN. It is clear that it is only the starburst systems which extend to redshifts in excess of 2. For those systems with redshifts less than 2, we have compared the redshift distributions for each classification.

The AGN and unclassified systems have median redshifts of 0.91 and 0.85 respectively, and a Kolmogorov-Smirnov goodness of fit test shows that there is a 79 per cent probability that they are drawn from the same population. Conversely, the starburst systems have a significantly lower median redshift of 0.56 and there is only a 7 per cent probability that they are drawn from the same population as the AGN systems. Thus it appears that majority of the starburst systems are associated with galaxies at a lower redshift than the AGN sources. On this basis, the majority of the unclassified sources are most likely to be AGN dominated systems with some starbursts included. It is worth noting, however, that nearly half the starburst systems appear in two adjacent histogram bins covering  $0.3 \leq z < 0.7$ . The excess of sources in these bins is correlated with the redshifts of two major clusters found by Cohen et al. (2000) in their Caltech Faint Galaxy Redshift Survey of the HDF.

The histogram of starburst galaxies and starburst candidates also shows evidence for a tail extending to redshifts in excess of 4 (although the highest redshift candidate may also contain an AGN). Fig. 9 shows that many of these high redshift starburst systems have been identified as sub-mm sources (Chapman et al. 2004a, Chapman et al. 2004c submitted). In addition, two are optically faint and extremely red, suggesting that they are dust-enshrouded. Of the thirteen optically faint radio sources in the 10-arcmin field, only two are classified as AGN or AGN candidates. Thus, although the majority of starburst systems are associated with galaxies brighter than  $I = 25$  and at redshifts less than two, it appears that we are beginning to sample an additional population of high redshift systems. In addition, some of these high redshift systems may be complex, containing both dust-shrouded starbursts and embedded AGN (see Appendix B and Section 9).

### 7.3 Structural classification and source flux density

Fig. 7 summarises the classification of the 92 sources in the 10-arcmin field in each of three flux density ranges ( $40\text{--}55 \mu\text{Jy}$ ,  $56\text{--}105 \mu\text{Jy}$ , and  $106\text{--}6000 \mu\text{Jy}$ ); these contain approximately equal numbers of sources: 30, 30, and 32 respectively. It is immediately apparent that the proportion of starburst and starburst candidate systems rapidly increases with decreasing flux density below  $100 \mu\text{Jy}$ . In the highest flux density range, there are only around 20 per cent starburst systems with around 40 per cent AGN and 40 per cent unclassified sources. In the lowest flux density range, the proportion of starburst systems has risen above 70 per cent while the proportion of AGN systems has dropped to less than 5 per

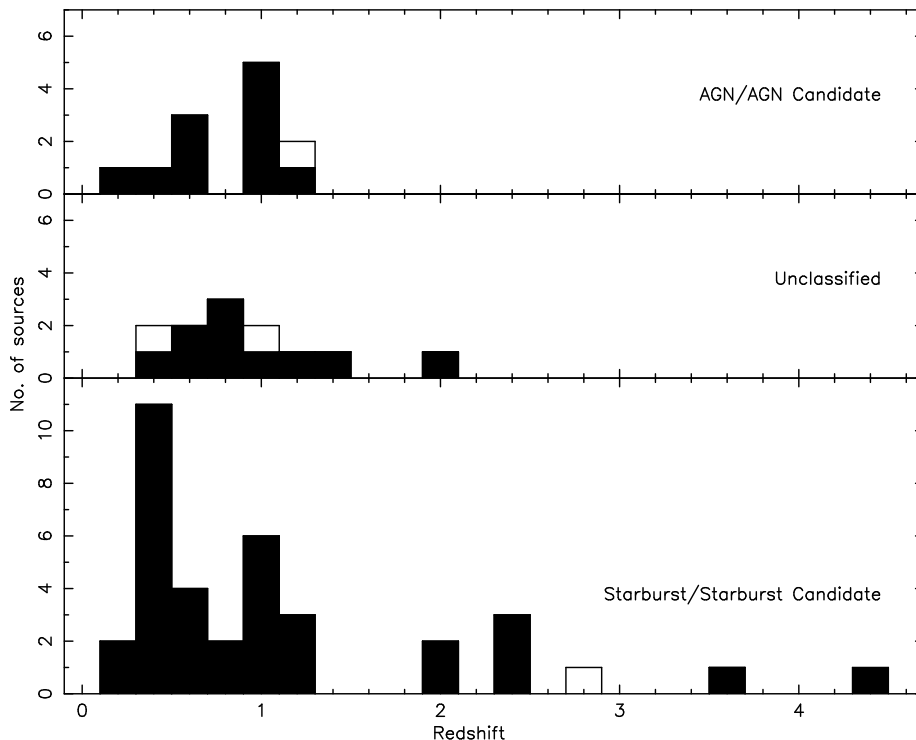


**Figure 6.** Redshift distribution for those sources in the 10-arcmin field with measured spectroscopic redshifts (black) and estimated photometric redshifts (white).

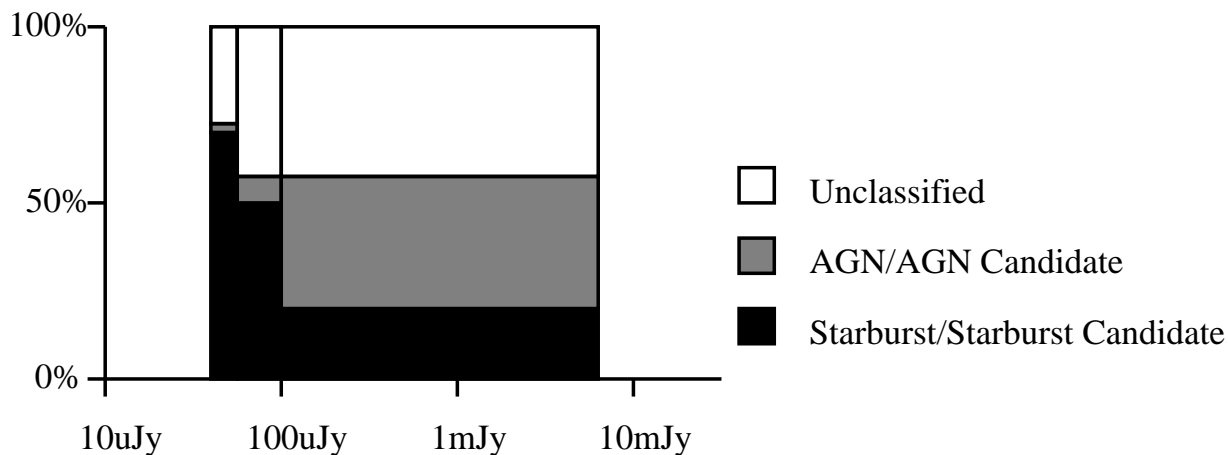


**Figure 7.** Distribution of source classifications for the objects in the 10-arcmin field in each of three flux ranges ( $40\text{--}55 \mu\text{Jy}$ ,  $56\text{--}105 \mu\text{Jy}$ , &  $106\text{--}6000 \mu\text{Jy}$ ) containing 30, 30, & 32 sources respectively.

cent. Fomalont et al. (2002) note that in their sample of radio sources at 8.4 GHz, the average radio spectrum for those sources identified with optical counterparts becomes steeper for fainter sources ( $S_{8.4} < 35 \mu\text{Jy}$ ). These authors also state that objects fainter than  $I = 25.5$  mag predominantly have steep radio spectra. Thus it is clear that at flux densities below around  $50 \mu\text{Jy}$  at centimetric wavelengths, a popu-

lation of steep radio spectrum starburst systems begins to dominate.

There is, however, a selection effect which could reduce the numbers of AGN identified at low flux levels. AGN systems are easily identified if they have flat or inverted radio spectra. Radio spectral information is derived from the present 1.4-GHz observations and those at 8.4 GHz

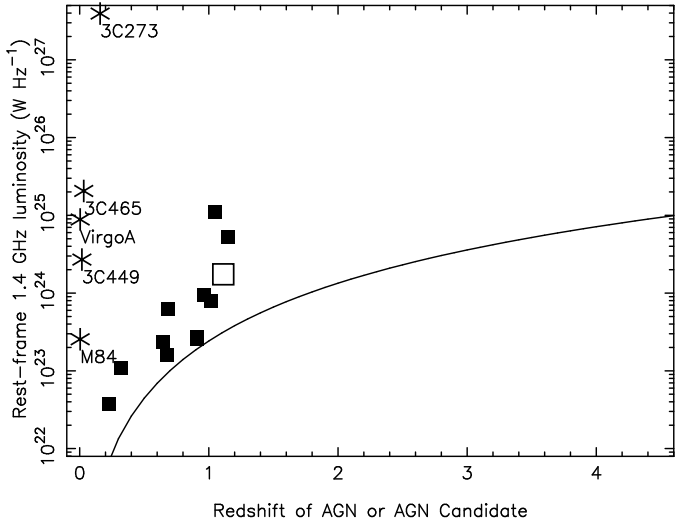


**Figure 8.** 1.4-GHz monochromatic luminosity for AGN and AGN candidate sources with redshifts in the 10-arcmin field. Filled symbols are spectroscopic redshifts, open symbols are photometric redshifts. Asterisks show named sources. The plotted line marks the detection threshold of  $40 \mu\text{Jy}$  for sources assuming a spectral index of 0 ( $\Omega_V = 0.7$ ,  $\Omega_M = 0.3$ , and  $H_0 = 65 \text{ km s}^{-1} \text{ Mpc}^{-1}$ ).

(Richards et al. 1998). The 8.4-GHz image is extremely sensitive (rms noise =  $2.78 \mu\text{Jy beam}^{-1}$ ); however the small primary beam of the VLA antennas (HPBW = 5.2 arcmin) restricts the region of source detection to a field of around 8 arcmin in diameter. Weak sources close to the edge of the 10-arcmin field will not be detected at 8.4 GHz, and this is likely to prevent the correct identification of weak AGNs. Such systems are likely then to be designated as ‘unclassified’. However, since less than 20 per cent of the unclassified sources are found in the lowest flux range shown in Fig. 7, it is thought that few if any AGN have been mis-identified at low flux levels. Moreover the  $K$ -correction works in favour of detecting AGN in comparison with starbursts at high  $z$ , as noted in Section 8.2.

#### 7.4 Source luminosities and star-formation rates

Figs. 8 and 9 show the rest-frame 1.4-GHz monochromatic luminosities for the AGN, and starburst/starburst candidate sources in the 10-arcmin field with measured or estimated redshifts respectively, together with a number of well-known lower redshift radio sources of each type. The detection threshold for  $40 \mu\text{Jy}$  is plotted as a line assuming a radio spectral index of 0 for the AGNs and 0.7 for the starburst systems.

All the AGN candidates are well above the detection threshold which simply reflects the fact that they have flux densities well above  $40 \mu\text{Jy}$ . Their luminosities are similar to those of low luminosity, low redshift FRI type radio galaxies like M84, Virgo A, and 3C449 (Fanaroff & Riley, 1974); but significantly lower than those of FRII type sources and powerful quasars like 3C273 (see Fig. 8 where the source 3C465 has a rest-frame luminosity intermediate between FRI and FRII type systems). However, apart from two sources (J123644+621133 and J123725+621128) which show ‘classi-

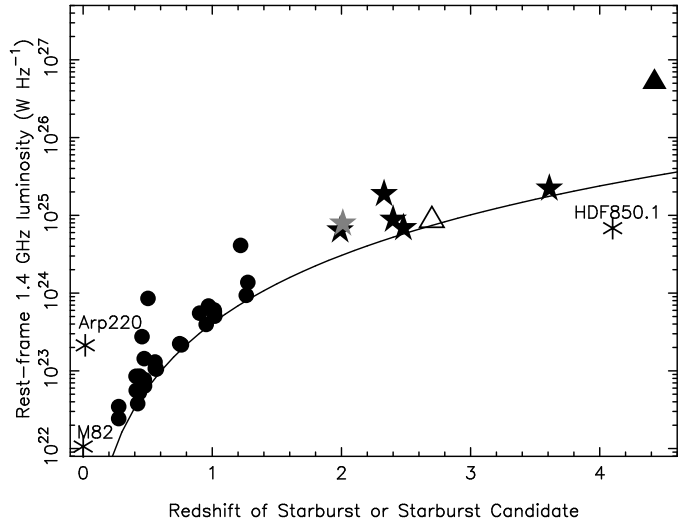


**Figure 9.** 1.4-GHz monochromatic luminosity for starburst and starburst candidate sources with redshifts in the 10-arcmin field. Filled symbols are spectroscopic redshifts, open symbols are photometric redshifts. Five-pointed stars mark sub-mm systems. Triangles mark two high redshift systems with possible embedded AGN, (J123642+621331, & J123651+621221). The sub-mm system with a possible embedded AGN (J123635+621424) is shown in grey. Asterisks show named sources. The plotted line marks the detection threshold of  $40 \mu\text{Jy}$  for sources assuming a spectral index of 0.7 ( $\Omega_V = 0.7$ ,  $\Omega_M = 0.3$ , and  $H_0 = 65 \text{ km s}^{-1} \text{ Mpc}^{-1}$ ).

cal’ double radio structures, all the remaining AGN systems are small core-jet systems extended on sub-galactic scales.

The starburst candidates lie closer to the detection threshold since they represent the majority of the weaker radio sources in the 10-arcmin field. All the systems are substantially more powerful than M82 and about half are more luminous than Arp 220. The sources at  $z > 2$  (marked as stars and triangles in Fig. 9) have particularly high luminosities exceeding that of Arp 220 by an order of magnitude. The object at the highest redshift (J123642+621331) which is more than 3 orders of magnitude more luminous than Arp 220, may be a hybrid system containing both a dust-shrouded starburst and an embedded AGN (see discussion in Appendix B). The other two starburst sources which appear to contain compact AGN are not noticeably super-luminous. Star-formation rates for starburst and starburst candidate systems with measured redshifts are shown in Table 3. These are derived from the rest-frame monochromatic 1.4-GHz luminosity via the relationship derived by Condon & Yin (1990) and Condon (1992). Star-formation rates for stellar masses  $> 5 M_\odot$  were calculated using the relationships given by Cram et al. (1998) and then multiplied by 5.5 to give the total star-formation rate for stellar masses between  $0.1 M_\odot$  and  $100 M_\odot$  using a Salpeter IMF.

## 8 COMPARISON WITH OTHER CATALOGUES

### 8.1 The WSRT catalogue

After our data had been taken and analysed, it has become clear that a number of extended, low surface-brightness radio

**Table 3.** Rest-frame monochromatic 1.4-GHz Luminosities and star-formation rates (assuming Salpeter IMF, see Section 7.4) for starburst systems with measured or estimated redshifts. Star-formation rates marked with an \* may be overestimates as these galaxies are thought to contain an embedded AGN.

Name	L <sub>1.4</sub> (W Hz <sup>-1</sup> )	Redshift	Approximate Star-formation Rate (M <sub>⊙</sub> yr <sup>-1</sup> )
J123606+621021	1.9 × 10 <sup>25</sup>	2.33	4400
J123607+621328	5.2 × 10 <sup>22</sup>	0.4353	12
J123608+621553	7.0 × 10 <sup>22</sup>	0.4593	16
J123612+621138	2.4 × 10 <sup>22</sup>	0.275	6
J123612+621140	3.5 × 10 <sup>22</sup>	0.275	8
J123615+620946	9.4 × 10 <sup>23</sup>	1.263	220
J123616+621513	2.2 × 10 <sup>25</sup>	3.61	5100
J123619+621252	1.4 × 10 <sup>23</sup>	0.473	34
J123621+621109	6.1 × 10 <sup>23</sup>	1.014	140
J123622+621629	8.7 × 10 <sup>24</sup>	2.40	2000
J123622+620945	2.2 × 10 <sup>23</sup>	0.7479	42
J123630+620923	4.0 × 10 <sup>23</sup>	0.953	93
J123632+621700	8.5 × 10 <sup>22</sup>	0.437	20
J123633+621005	5.8 × 10 <sup>23</sup>	1.016	135
J123634+621213	2.7 × 10 <sup>23</sup>	0.456	64
J123634+621241	4.1 × 10 <sup>24</sup>	1.219	960
J123635+621424	7.8 × 10 <sup>24</sup>	2.011	1800
J123642+621331	5.2 × 10 <sup>26</sup>	4.424	120000*
J123646+621629	8.5 × 10 <sup>23</sup>	0.502	200
J123646+620833	6.8 × 10 <sup>23</sup>	0.9712	160
J123649+621313	6.4 × 10 <sup>22</sup>	0.475	15
J123650+620801	1.1 × 10 <sup>23</sup>	0.559	25
J123650+620844	8.1 × 10 <sup>22</sup>	0.434	19
J123651+621030	8.5 × 10 <sup>22</sup>	0.410	20
J123651+621221	8.6 × 10 <sup>24</sup>	2.7	2000*
J123653+621139	1.4 × 10 <sup>24</sup>	1.275	320
J123656+621301	7.7 × 10 <sup>22</sup>	0.474	18
J123659+621449	2.2 × 10 <sup>23</sup>	0.761	51
J123705+621153	5.5 × 10 <sup>23</sup>	0.902	130
J123707+621408	6.8 × 10 <sup>24</sup>	2.48	1600
J123708+621056	3.8 × 10 <sup>22</sup>	0.422	9
J123711+621325	6.4 × 10 <sup>24</sup>	1.99	1500
J123714+621558	1.1 × 10 <sup>23</sup>	0.567	25
J123716+621643	1.3 × 10 <sup>23</sup>	0.557	30
J123716+621007	5.6 × 10 <sup>22</sup>	0.411	13
J123721+621346	5.0 × 10 <sup>23</sup>	1.019	120

sources may have been missed by the initial VLA-only finding survey. Using the WSRT interferometer, which has much lower angular resolution (15 arcsec) and is thus more sensitive to extended objects than the VLA A-array (2-arcsec resolution), Garrett et al. (2000) detect additional radio sources in the region of the 10-arcmin field. Furthermore, they identify at least two (J123720+621247 and J123636+621132) with nearby, extended star-forming galaxies. Since these objects were not detected by the VLA, it implies they are extended on the 5 – 20 arcsec angular scale and do not contain compact radio structure. However, the crowded nature of the optical field makes identification for most of these new detec-

tions very uncertain. In addition, Garrett et al. (2000) state that further analysis of the full field is required to distinguish how many of the WSRT-only detections are real and associated with discrete, extended radio sources, and how many are blends of closely-separated, faint radio sources.

The WSRT source catalogue given by Garrett et al. (2000) lists 85 objects above a 5 $\sigma$  limit of  $\sim 50 \mu\text{Jy}$  within the 10-arcmin field. Of these 63 are also detected by the VLA hence 22 are WSRT-only detections. The VLA-only flux densities listed in Table A2 include 78 sources above 50  $\mu\text{Jy}$  (6.7 $\sigma$ ) of which 15 are VLA-only detections. One possible explanation is that these sources have varied between

the epochs of the VLA and WSRT observations. However, many of the VLA-only detections show extended radio structures in the MERLIN+VLA combination images and have steep radio spectra – indeed, in Section 7, we argue that the majority of weakest radio sources in the 10-arcmin field are extended starburst systems. These objects are very unlikely to be variable radio sources. The implication is that the WSRT catalogue is unreliable at this level, and that of the 22 WSRT-only detections, perhaps only between 8 and 10 are real extended low-surface brightness radio sources lying within the 10-arcmin field which have been missed by the VLA. It is still likely, therefore, that the VLA-based source list in Table A2 is incomplete and is missing  $\sim 10$  per cent of the  $\mu\text{Jy}$  radio source population.

## 8.2 ISO

Aussel et al. (1999) detected 100 sources at 6.7 or 15  $\mu\text{m}$  or both within the HDF/HFF. The *ISO* beams were 3 and 6 arcsec within  $\sim 3.5$  and  $\sim 5$  arcmin fields of view at the shorter and longer wavelengths respectively; 28 radio sources lie within the maximum *ISO* field of view. Of these, 15 have IR counterparts within 3 arcsec. In addition the core of the FRI J123644+621133 is just over 3 arcsec from a 6.7- $\mu\text{m}$  source, found only by the *ISO* detection method described by Goldschmidt et al. (1997). Two more (J123646+621445 and J123656+621301) are at separations of 3–6 arcsec; in the case of J123646+621445 the IR source appears to be associated with a separate nearby galaxy (see Appendix B). Note that in the column in Table A2 labelled *ISO*, ‘–’ signifies that the source is outside the *ISO* field and ‘No’ signifies a non-detection within the field at the local flux-density limit, see Aussel et al. (1999) for details of how this varies with position and frequency. Twelve of the radio sources with IR counterparts are classified as starburst galaxies using the criteria in Section 5.1 (of which 3 have embedded AGN), two are AGN and two are unclassified. The majority of radio sources (7) within the *ISO* field of view which do not have IR counterparts are also starburst candidates, 3 are unclassified and 2 are AGN/AGN candidates.

Starbursts typically have a steep spectrum in both the IR and the radio whilst AGN have a flatter radio spectrum. Hence the *K*-correction implies that, at the same luminosity, AGN should be detectable at greater distances than starbursts and the proportion of the latter may be underestimated. Elbaz et al. (2002) showed that 80 – 90 per cent of the extragalactic 15  $\mu\text{m}$  background is of starburst origin and 3/4 of ISOCAM galaxies are ULIRGs (Ultra-Luminous IR Galaxies). The proportions are consistent in other deep surveys such as of the Lockman Hole as well as in the HDF.

Garrett (2002) demonstrated that the 1.4-GHz and 15- $\mu\text{m}$  rest-frame luminosities of HDF sources detected by both WSRT and *ISO* are closely correlated out to at least  $z \sim 1.3$ , suggesting a common emission environment. This correlation is based on using a starburst-model spectral index in the IR and the vast majority of the radio sources with associated IR emission are independently classified as starburst candidates. A third of the radio sources in the sample identified by Garrett (2002) are among the non-detections seemingly resolved-out in the MERLIN+VLA data (Section 8.1). One may be a misidentification and 10 out of the 12 remaining

sources have extended emission and other starburst characteristics.

73 *ISO* sources lie within the 3-arcmin field. In order to investigate statistical associations with the *ISO* sources, the mean MERLIN+VLA flux density from within concentric circles centred on the *ISO* positions was measured, together with equivalent flux densities of a control sample incorporating a 10-arcsec random position offset from the radio position. The most significant correlation with the radio brightness is obtained with circles of 2.5 arcsec diameter. The results are shown in Fig. 10 and we note that radio flux densities  $> 10 \mu\text{Jy}$  were found at the positions of 30 *ISO* detections, about half of which are probably significant statistically. Although this is only a  $\sim 2\sigma$  result it indicates that deeper surveys and more accurate IR positions, as will be obtained with the *Spitzer* satellite, are likely lead to many more radio-IR associations.

## 8.3 Chandra

43 of the 92 sources in the 10-arcmin field sample (47 per cent) were detected in X-rays by *Chandra* using a 1 Ms exposure (Hornschemeier et al. 2001). A further 12 counterparts with full-band counts  $< 65$  were found in the full 2 Ms *Chandra* exposure recently catalogued by Alexander et al. (2003). These are all listed in Table A2. Note that in the column labelled *Chandra*, ‘No’ signifies a non-detection within the field at the local flux-density limit, see Alexander et al. (2003) for details of how this varies with position and energy. The *Chandra* field of view at high sensitivity is slightly larger than the 10-arcmin radio field.

We note that the X-ray detection rate appears to be uncorrelated with the radio source flux density since in each of the three flux ranges shown in Fig. 7, 16/30, 20/30, and 19/32 radio sources are detected by *Chandra* respectively. In addition, Fomalont et al. (2002) state that the seven X-ray identifications (from the 1 Ms observation) in the HDF itself show no trends in radio spectral index or optical counterpart and are identified with galaxies of various spectral types. There is no obvious correlation between X-ray and radio flux densities or classification. Since Fig. 7 shows that source classification is a strong function of radio flux density, this implies that the X-ray emission from the  $\mu\text{Jy}$  radio source population is not a good predictor of AGN activity in the HDF unless this arises from a separate mechanism within the same galaxy.

A long series of papers have appeared analysing the *Chandra* results using multi-wavelength comparisons. However thus far most considerations of radio data have used the 1 Ms X-ray catalogue and the VLA-only radio data. In the next paper we intend to use Virtual Observatory tools to compare the new more sensitive samples which, for the first time, contain enough sources in common to allow comparisons based on selection by specific properties such as spectral index or redshift.

## 8.4 SCUBA sub-mm sources

Identifying the optical/NIR counterparts to sub-mm sources has proved difficult due to the poor spatial resolution and astrometric capability of current sub-mm telescopes. However, high resolution radio images offer new possibilities for

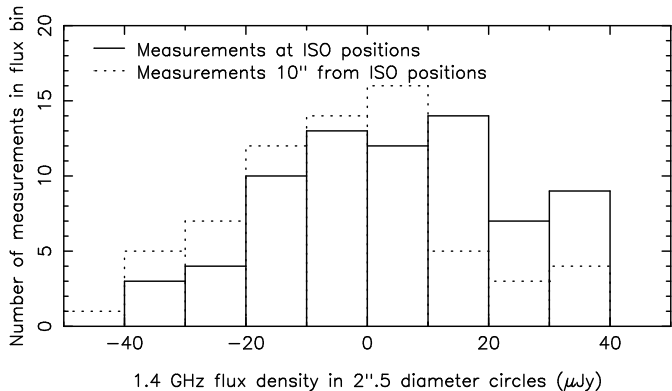


**Figure 10.** Histogram showing the MERLIN+VLA 1.4-GHz brightness at the positions of *ISO* detections within the 3' field, compared with the off-source brightness. The 'on source' histogram is shifted to the right of the 'off source' one indicating a weak statistical association of radio emission with *ISO* sources.

locating sub-mm sources and for the determination of their properties. For starburst systems, it is well established that the radio continuum flux (due to synchrotron emission from SNR and violent turbulence associated with intense star-formation) and the FIR/sub-mm flux (due to dust from stellar winds) are tightly correlated as a result of their both being linearly related to the massive star-formation rate (e.g. Helou et al. 1985, Helou & Bicay, 1993). If the FIR-radio correlation extends to high redshift then in principle, sensitive radio observations can be used to pinpoint distant sub-mm sources.

From radio-far-infrared SED-based redshift arguments Smail et al. (2000) have suggested that the median redshift for the bright SCUBA galaxy population is  $\sim 3$ , with the substantial majority of SCUBA sources lying at redshifts  $> 2$ . Dunlop et al. (2004) argue that since SCUBA sources in other fields have been identified with relative ease compared with HDF850.1 (see below), the majority probably lie at redshifts  $< 4$ . This is in agreement with Hughes et al. (1998) who have assumed a redshift range of  $2 < z < 4$  for calculating the contribution made by sub-mm sources to star-formation density. Ivison et al. (2002) have investigated the SCUBA source population in the Lockman Hole and ELAIS N2 regions with deep multi-band imaging. With good radio positional information, they identify radio counterparts for 18 of 30 sub-mm sources. Of these, they find that at least 60 per cent of the host galaxies appear to be morphologically distorted, suggesting that the radio and sub-mm emission arises from extended starbursts and that interactions are common.

With all this in mind, and armed with our accurate radio-optical astrometry, we have revisited the issue of sub-mm source identifications in the HDF and HFF. We have used the results of Serjeant et al. (2003) who have re-measured the positions for the eight brightest sub-mm sources in a field centred on the HDF (Hughes et al. 1998). Following discussion with S. Serjeant on the sub-mm position errors, we have drawn error circles with a radius of  $2\sigma$  where  $\sigma = \sqrt{1^2 + \theta_{\text{SNR}}^2}$  arcsec. In this quadratic combination the first term is an estimate of the positional error due to confusion and the second is the standard random error due to finite signal-to-noise ratio ( $\theta_{\text{SNR}} = 0.5 \times \text{FWHM}/\text{SNR}$ ).

FWHM is the size of the imaging beam. Fig C2 shows these error circles overlaid on the astrometrically aligned optical fields. The combined MERLIN/VLA radio images at the position of each sub-mm source at 0.6-arcsec resolution are shown as contours. Following the assessment by Serjeant et al. of the sub-mm signal-to-noise ratio of HDF850.3, we are not convinced by its reality and therefore we do not include it.

We now discuss the individual sub-mm sources in, or close to the edge of, the HDF as presented by Serjeant et al. (2003). Our discussion draws extensively on that of Serjeant et al.; however in a number of cases we come to different conclusions as a result of the improved radio information that we have at our disposal.

#### 8.4.1 HDF850.1

The suggested association of Serjeant et al. for this source is the elliptical galaxy 3-586.0 (Williams et al. 1998), although they do allow the possibility that HDF850.1 is optically faint. The astrometric alignment of the optical field to the ICRF (derived from radio observations presented here), together with observations by IRAM (again with respect to the ICRF) has now allowed Dunlop et al. (2004) unambiguously to identify this brightest sub-mm source. Dunlop et al. have shown that, in a Subaru *K'* band image, from which a smoothed version of WFPC2 *I*-band frame has been subtracted, there is an extremely red object (ERO) with  $I-K > 5.2$  at the position of a very weak ( $16 \mu\text{Jy}$ ) radio source which lies  $\sim 1$  arcsec to the SW of the elliptical galaxy 3-586.0. The radio source/ERO is within the  $3\sigma$  positional errors as measured by the IRAM interferometer (Downes et al. 1999) on the ICRF system. The SED determined by Dunlop et al. suggests the ERO is a starburst system at a redshift of  $4.1 \pm 0.5$ . The inferred star formation rate is very high ( $\sim 2000 M_{\odot} \text{ yr}^{-1}$ ), although this may be reduced by a factor close to 3 after correction for gravitational lens boosting by the intervening elliptical galaxy  $\sim 1$  arcsec to the NE.

#### 8.4.2 HDF850.2

The SCUBA source lies just outside the HDF and hence we reproduce the CFHT optical field; there is no optical candidate down to  $I \sim 25$  mag within the error circle. The nearest optical galaxy is 36564+1209 ( $I \sim 23$  mag, Barger et al. 1999) which lies 5.6 arcsec to the north of the SCUBA position. The extended, steep-spectrum radio source J123656+621207 ( $46 \mu\text{Jy}$ ,  $\alpha > 1.32$ ) lies 4.2 arcsec to the north of the SCUBA position, outside the error circle. The radio source and the optical galaxy are certainly not coincident. It remains possible, although in our view unlikely, that the radio source J123656+621207 is associated with the sub-mm source. Whether the SCUBA source is associated with J123656+621207 or not, it is clearly associated with an optically faint system, below the limit of the CFHT or WFPC2 images of this HFF field.

#### 8.4.3 HDF850.4

HDF850.4 and HDF850.5 are a possible blended detection. Borys et al. (2003) in a reworking of the sub-mm data list

this as a single detection (SMJ123650+621318). After consultation with S. Serjeant we have treated HDF850.4 and HDF850.5 as separate sub-mm detections but for completeness we have also plotted an error circle derived for the blended source position from Borys et al. (see above).

Serjeant et al. (2003) suggest that HDF850.4 may be associated with the  $z = 0.851$  (Cowie et al., 2004) galaxy 2-339.0 which lies within 0.8 arcsec of the sub-mm source position and close to the centre of the field as reproduced. However, Carilli & Yun (1999) argue that this is hard to reconcile with the lack of any detected radio emission with an Arp 220-like SED since at this redshift they would expect  $S_{1.4} \sim 280 \mu\text{Jy}$ . There is a  $3\sigma$  radio detection of  $14 \mu\text{Jy}$  close to the nuclear region of 2-339.0. However, this radio flux density is still less than 1/20 of that predicted by Carilli & Yun (1999) for an Arp 220-type SED at  $z = 0.9$ . We note that this galaxy lies within the error circle associated with SMMJ123650+621318 (Borys et al. 2003).

Another possible identification is with the bright  $I = 21.1$  mag galaxy 2-264.1 ( $z = 0.475$ ) coincident with the high signal-to-noise ratio radio source J123649+621313 ( $S_{1.4} = 49 \mu\text{Jy}$ ) which is listed as a starburst system in Table A2. This galaxy lies 5.3 arcsec to the SW and within the error circle.

For completeness one should also consider the  $I = 22.7$  mag ( $z = 1.238$ ) galaxy which lies just outside the error circle  $\sim 6$  arcsec to the west of the sub-mm position as a candidate identification. This galaxy also contains a radio source ( $S_{1.4} \sim 27 \mu\text{Jy}$ ). In addition, another candidate radio identification lies close to the southern edge of the error circle. The  $S_{1.4} \sim 19 \mu\text{Jy}$  possible radio detection is not associated with any optical object to the limit of the CFHT image.

The identification of this sub-mm source remains unclear.

#### 8.4.4 HDF850.5

Serjeant et al. (2003) state that the position of this source is likely to have been affected by the proximity of HDF850.4 (see also above). The most obvious optical candidate, galaxy 2-404.0 ( $z = 0.199$ , Lanzetta et al. 1996), lies 6.6 arcsec to the west but is not a radio source.

Our deep radio image shows a possible radio counterpart on the eastern edge of the error circle at the  $3\sigma$  level ( $14 \mu\text{Jy}$ ). There is no optical identification at this radio position to the limit of the *HST* WFPC2 image.

We concur with Serjeant et al. who conclude that there is no reliable identification for this object.

#### 8.4.5 HDF850.6

This source lies outside the HDF and we reproduce both the WFPC2 and CFHT images of this region in the HFF. Serjeant et al. (2003) suggest that this object is most likely to be associated with the radio source J123701+621146 ( $S_{1.4} = 128 \mu\text{Jy}$ ) which we classify as a starburst in Table A2. The radio source lies 2.9 arcsec from the sub-mm position but is within the error circle. Although the source is extended over  $\sim 3$  arcsec in the VLA-only image, a high resolution image shows that the central 1.5 arcsec overlies

an ERO with  $I-K > 5$  (Alexander et al. 2001). This is not visible in the *HST* WFPC2 frame, but is just detectable in the lower resolution CFHT image which has a better surface brightness sensitivity. Cohen et al. (2000) derive a spectroscopic redshift of  $z = 0.884$  for the ERO on the basis of a single detected emission line ( $\text{O II}, \lambda_{3727}$ ).

In agreement with Serjeant et al. we conclude that J123701+621146 is the most likely radio counterpart to HDF850.6 and is probably identified with the ERO and the SCUBA source. There is however one other possible radio detection ( $15 \mu\text{Jy}$ ) lying within the error circle, but this has no optical counterpart to the limits of either of the WFPC2 HFF or CFHT images. If this latter radio source is the correct association, the radio to sub-mm flux ratio would imply a redshift  $z \geq 4$  (see discussion in Section 8.6).

#### 8.4.6 HDF850.7

Serjeant et al. (2003) discuss a possible identification of this source with a  $z = 1.219$  (Barger et al. 1999)  $I = 22.3$  mag galaxy which lies  $\sim 5$  arcsec from the sub-mm position just outside the error circle. This galaxy is identified with the steep-spectrum radio source J123634+621241 ( $S_{1.4} = 230 \mu\text{Jy}$ ). Our high resolution image of this radio source confirms that it is an extended starburst system (Table A2). The galaxy is also detected in X-rays by *Chandra* and is identified with the *ISO* source HDF\_PM3\_3 (Aussel et al. 1999).

Although the positional offset gives a relatively high probability of a chance coincidence with J123634+621241, Serjeant et al. argue that this source lies in a noisy area of the SCUBA image, and that the positional errors may have been underestimated. Our radio image shows only one other possible detection within the error circle ( $3\sigma$ ,  $15 \mu\text{Jy}$ ) for which there is no optical counterpart to the limit of the *HST* WFPC2 image. We conclude that the galaxy identified with J123634+621241 is the most likely optical counterpart to HDF850.7, but the positional offset makes this identification far from certain. By analogy with HDF850.1, the weak radio detection cannot be discounted.

#### 8.4.7 HDF850.8

Serjeant et al. (2003) suggest that the galaxy 2-736.1, the eastern-most member of an interacting pair of galaxies  $\sim 2$  arcsec from the sub-mm position, is the most likely identification for this source. Cohen et al. (2000) measure a spectroscopic redshift of  $z = 1.355$  for this galaxy.

Our radio image shows a weak ( $\sim 15 \mu\text{Jy}$ ) source associated with 2-736.1, although it is offset to the south-east by  $\sim 0.5$  arcsec from the optical centroid. The radio to sub-mm flux ratio suggests a higher redshift ( $\sim 2$ ) than that measured, although the uncertainties are large. Although this remains the most plausible identification for HDF850.8, there are a number of other possible radio sources lying within the SCUBA error circle (including a  $23\text{-}\mu\text{Jy}$  source on the western edge) which cannot be discounted. None, however, have optical counterparts to the limit of the *HST* WFPC2 image.

**Table 4.** Candidate radio source identifications above  $4\sigma$  in the region of each sub-mm detection as listed by Serjeant et al. (2003)<sup>•</sup>, Chapman et al. (2004b)<sup>◦</sup>, and Borys et al. (2003)<sup>†</sup>. For Borys et al. (2003) we include only those sub-mm detections above  $5\sigma$  not already listed by either Serjeant et al. (2003) or Chapman et al. (2004b). Furthermore, for Borys et al. (2003), since the nominal error circles are relatively large, we include only those radio candidates above  $5\sigma$ . Sources marked with an \* are possible bright ( $S_{1.4} > 40 \mu\text{Jy}$ ) radio counterparts which lie just outside the nominal sub-mm positional error circle as described in Section 8.4 and shown in Fig C2. The radio images were restored with a circular beam of 0.6 arcsec prior to cross-referencing with the sub-mm position. Redshift shown bracketed are uncertain due to significant radio/sub-mm position offsets.

Sub-mm Name	$S_{850}$ $\mu\text{Jy}$	R. A. Radio	Dec.	Peak Radio Brightness $\mu\text{Jy beam}^{-1}$	Redshift
HDF850.1 <sup>•</sup>	5.6	12:36:52.060	+62:12:25.67	16	4.1
HDF850.2 <sup>•</sup>	3.5	12:36:56.5566	+62:12:07.425	31*	
HDF850.4 <sup>•</sup>	1.1	12:36:49.455	+62:13:16.66	20*	1.238
		12:36:49.7432	+62:13:13.065	27	0.475
		12:36:50.479	+62:13:16.10	14	0.851
		12:36:50.647	+62:13:10.84	19	
HDF850.5 <sup>•</sup>	1.0	12:36:52.852	+62:13:18.50	14	
HDF850.6 <sup>•</sup>	6.4	12:37:01.021	+62:11:45.86	14	
		12:37:01.5745	+62:11:46.814	34	
HDF850.7 <sup>•</sup>	5.5	12:36:34.5168	+62:12:41.107	101	1.219
		12:36:34.812	+62:12:41.57	15	
HDF850.8 <sup>•</sup>	1.7	12:36:52.393	+62:13:54.82	23	
		12:36:52.845	+62:13:54.00	15	1.355
		12:36:52.907	+62:13:52.07	13	
		12:36:52.985	+62:13:57.97	14	
		12:36:53.123	+62:13:56.58	14	
SMMJ123606.9+621021 <sup>◦</sup>	11.6	12:36:06.8493	+62:10:21.437	33	2.33
SMMJ123616.2+621514 <sup>◦</sup>	5.8	12:36:16.1419	+62:15:13.937	32	3.61
SMMJ123618.3+621551 <sup>◦</sup>	7.3	12:36:18.3353	+62:15:50.585	110	(1.87)
SMMJ123621.3+621708 <sup>◦</sup>	7.8	12:36:21.2691	+62:17:08.458	116	(1.99)
SMMJ123622.7+621630 <sup>◦</sup>	7.7	12:36:22.653	+62:16:29.71	25	2.40
SMMJ123629.1+621046 <sup>◦</sup>	5.0	12:36:29.124	+62:10:45.98	23	1.013
SMMJ123635.6+621424 <sup>◦</sup>	5.5	12:36:35.5839	+62:14:24.049	44	2.011
SMMJ123646.1+621449 <sup>◦</sup>	10.3	12:36:46.0629	+62:14:48.713	91	
SMMJ123707.2+621408 <sup>◦</sup>	4.7	12:37:07.2209	+62:14:08.208	31	2.48
SMMJ123712.0+621325 <sup>◦</sup>	4.2	12:37:11.9865	+62:13:25.771	39	1.99
SMMJ123622+621618 <sup>†</sup>	8.6	12:36:22.279	+62:16:15.57	23	
SMMJ123634+621409 <sup>†</sup>	11.2	Not Detected		<22	
SMMJ123637+621157 <sup>†</sup>	7.0	Not Detected		<22	
SMMJ123703+621303 <sup>†</sup>	3.4	12:37:03.352	+62:13:06.15	23	

### 8.5 Other sub-mm samples

Chapman et al. (2004c, submitted) have compiled a sample of sub-mm sources lying within a 7.5-arcmin diameter field centred on R. A.  $12^{\text{h}} 36^{\text{m}} 48^{\text{s}} 0$  Dec.  $+62^{\circ} 15' 40'' 0$  (J2000), which have  $S_{850} > 4$  mJy and are detected at 1.4 GHz in the VLA A-array observations of this region with  $S_{1.4} > 40 \mu\text{Jy}$  (Richards 2000). This field centre lies 162 arcsec north and 10 arcsec east of the HDF and 10-arcmin field pointing centre. Ten objects are common to both the sub-mm sample and the 10-arcmin radio field.

In Table 4 we list all the candidate radio source/sub-mm identifications for Serjeant et al. (2003) and Chapman et al. (2004b). For completeness we also note that Borys et al. (2003) have reworked a large amount of sub-mm data in a field which includes the HDF and parts of the HFF. From their list of detections we have selected those with a sub-mm signal-to-noise ratio  $> 5$  which are not included in

Serjeant et al. (2003) and Chapman et al. (2004b). These are listed in Table 4 together with any radio detections with a radio signal-to-noise ratio  $> 5$  falling within an error circle of radius  $1\sigma$  obtained using figure 4 in Borys et al. (2003). These are the most plausible associations but the large sub-mm positional errors listed by Borys et al. (2003) (typically  $\sigma = 4 - 5$  arcsec) do not allow unambiguous identifications to be made.

### 8.6 The radio sub-mm connection

We have been able to combine the deepest 850-micron SCUBA images of the HDF and HFF and the deepest, high resolution, 1.4-GHz radio images, both with the best available astrometric accuracy. Despite this only one sub-mm source, HDF850.1, can be unambiguously paired-up with a radio source. The over-riding reason for this state-of-affairs remains the present-day sub-mm resolution and astrometric



accuracies (with the exception of HDF850.1, separately measured with the IRAM interferometer, Downes et al. 1999) which are inadequate for crowded fields. But this is not a complete explanation since in some cases there are no plausible radio candidates within conservative sub-mm error circles. Carilli & Yun (1999, 2000) and Barger et al. (2000) have shown that the SEDs of both local and high-redshift ULIRGs are similar, and that the ratio of the radio and sub-mm flux densities can be used to construct a rough redshift indicator. The inverse  $K$ -correction ensures that the sub-mm flux density varies little with redshift, while the radio flux density falls off with the inverse square law. Barger et al. in their figure 8 show that a galaxy with a sub-mm flux density of 6 mJy will not be detected in the radio at 40  $\mu$ Jy for a redshift  $>4$ . Hence, it is likely that our failure to detect radio counterparts for some of the sub-mm detections in the HDF and HFF is simply due to their large redshift.

For the brighter sub-mm sources contained in the Chapman et al. (2004b) sample, the positional errors are lower than for those of Serjeant et al. (2003) which has allowed them to link them with radio sources in the 10-arcmin field. For the seven of their sub-mm sources listed in Table 4 with unambiguous identifications, we find that the measured redshifts lie in range 1 to 4 with a mean of 2.26.

## 9 OPTICALLY FAINT RADIO SOURCES

13 of the 92 sources (14 per cent) in the 10-arcmin field are not identified to the limit of the optical fields over which they lie. Richards et al. (1999) have suggested a number of possibilities regarding the nature of the optically faint, unidentified  $\mu$ Jy radio source population:

(i) They are FRI or FRII radio galaxies at moderate redshift. However, this would mean that optical counterparts would have absolute magnitudes 6 magnitudes fainter than typical FRI or FRII radio galaxies which have  $I \sim 20$  mag. Furthermore, our new 0.2-arcsec resolution images do not have the appropriate radio morphology. We therefore reject this hypothesis.

(ii) They are displaced lobes of asymmetric sources. However, other  $\mu$ Jy radio sources consist of only a single component coincident with the optical counterpart, and the optically faint systems do not have radio structures which differ significantly. We therefore consider this hypothesis to be unlikely.

(iii) The optical counterpart may be at such a high redshift,  $z > 7$ , that it is an  $I$ -band dropout due to the Gunn-Peterson effect.

(iv) The optical counterpart may be obscured by dust – see the previous section on the radio sub-mm connection.

(v) They represent a new population of objects.

The last three possibilities remain to be tested. We can, however, make some comments based on three individual objects.

As noted in Section 7.2, of the thirteen optically faint systems in the 10-arcmin field, only two are classified as AGN or AGN candidates. Six are classified as starbursts or starburst candidates with the remaining five listed as unclassified. Subsequent to the HDF WFPC2 imaging, deep IR studies of two of the starbursts (J123642+621331 and

J123651+621221) have revealed very red objects and are now identified as high-redshift dust-obscured starburst systems. In addition deep  $K'$  band imaging with the Subaru 8-m telescope has revealed an extremely red object associated with a weak 16- $\mu$ Jy MERLIN+VLA 1.4-GHz radio detection at the position of the brightest SCUBA sub-mm source HDF850.1 (see Section 8.4.1 for a detailed description).

Waddington et al. (1999) detect a very red object at the position of J123642+621331 with NICMOS in  $J$ - and  $H$ -band and with the KPNO 4-m at  $K$ -band. On the basis of a single Ly $\alpha$  emission line at 6595 Å and the observed spectral energy distribution, they infer a redshift of 4.424, and argue that it is a distant starburst disc galaxy with a weak embedded AGN. The radio structure consists of a compact component together with emission extended over 0.4 arcsec and is thus consistent with this interpretation. Garrett et al. (2001) detect the compact component with the EVN at an angular resolution of 20 mas; this may be the steep-spectrum AGN core.

Dickinson (2000) finds a very red NICMOS detection at the position of J123651+621221. The spectral energy distribution implies a dust-shrouded starburst at a redshift close to 2.7 (Alexander et al. 2001). The source is a hard *Chandra* X-ray detection which Hornschemeier et al. (2001) interpret as an obscured QSO. However, the extended steep-spectrum radio structure suggests a dust-obscured starburst system with no evidence for any compact radio core. If there is an obscured QSO in this object which is responsible for the X-ray emission, it is not a significant radio source.

The nature of the remaining optically faint sources remains unclear, but from the radio structures seen in the MERLIN+VLA combination images, it seems likely that those classified as starburst candidates are most likely to be high-redshift dusty systems. These represent the first few detections of a new population of objects. A variety of explanations are possible, for example activity around young black holes at  $z > 10$ , perhaps resulting from Population III star clusters. Following Haiman, Dijkstra & Mesinger (2004), such objects could be detectable at a level of tens of  $\mu$ Jy at a high enough surface density to occur in these observations. Such possibilities underscore the vital role played by high resolution radio observations since they have high astrometric positional accuracy, show the detailed distribution of galactic radio activity, and do not suffer from dust obscuration. However, more sensitive observations, with higher angular resolution, in the IR and sub-millimetre bands are required to understand the true nature of these optically faint radio sources.

## 10 FUTURE DEVELOPMENTS

Using the same data and with the availability of enhanced computer power, we are extending the statistical study limited to the 3-arcmin field in this paper (see Section 6 and Fig. 5), to encompass the whole of the 10-arcmin field. This will form the basis of a future paper and will contain a statistical analysis of a mapped area over an order of magnitude larger than the 3-arcmin field. Very recently deeper *HST* ACS images have been released (Giavalisco et al 2004), which we will compare with the radio data. We do not wish to delay the present publication, since the new *HST* data

require astrometric alignment in order to have confidence in any further identifications of radio sources with faint optical galaxies.

With the development of *e*-MERLIN and the EVLA significantly more sensitive observations of the HDF and HFF will become feasible within a few years. When these broadband instruments come on line, imaging at 1.4 GHz will be a factor of five times more sensitive than now. Combination imaging with similar integration times to the present study will therefore yield rms noise levels  $\sigma_{e\text{-MERLIN+EVLA}} \sim 0.6 \mu\text{Jy beam}^{-1}$  in which radio sources like that associated with HDF 850.1, with a flux density of only  $16 \mu\text{Jy}$ , will be detected at the  $20\sigma$  level. The slope of the integral source counts below  $40 \mu\text{Jy}$  implies an increase in the number of radio sources by a factor of six in a sample complete to  $8 \mu\text{Jy}$  (equivalent to the  $40\text{-}\mu\text{Jy}$  selection limit in the present 10-arcmin field). To this limit in the 10-arcmin field, we will be able to image in excess of 500 radio sources. Above  $5 \mu\text{Jy}$  ( $8\sigma$  – equivalent to the  $27\text{-}\mu\text{Jy}$  limit in the 3-arcmin field) we will image around 1000 radio sources. Furthermore, the radio-optical statistical studies will be extended to radio sources with flux densities less than  $1 \mu\text{Jy}$ .

Compared with our current capabilities, at 5 GHz the imaging sensitivity will be increased by a factor of  $\sim 30$  within the inner 3-arcmin field (constrained by the Lovell telescope primary beam), and by a factor of  $\sim 15$  within a 9-arcmin field (constrained by the primary beams of the other antennas). This will result in noise levels of  $\sigma_{e\text{-MERLIN+EVLA}} \sim 0.15 \mu\text{Jy beam}^{-1}$  in the inner region and  $0.3 \mu\text{Jy beam}^{-1}$  in the outer combined with an angular resolution of  $\sim 50$  mas. Many of the starburst systems resolved for the first time in this work will thus be mapped with very high angular resolution, revealing the detailed areas of star-formation for the first time and detecting any embedded AGN compact cores. Together with the 5-GHz astrometric precision of a few mas, detailed cross-waveband comparisons of conditions within each galaxy will thus be possible.

## 11 SUMMARY AND CONCLUSIONS

### 11.1 Observational Results

In a 10-arcmin field centred on the HDF, a complete sample of 92 sources with flux densities above  $40 \mu\text{Jy}$  have been detected with the VLA, and imaged with the MERLIN+VLA combination at resolutions of 0.2, 0.3 and 0.5 arcsec (Table A1). These are amongst the most sensitive 1.4-GHz images yet made, with rms noise levels of  $3.3 \mu\text{Jy beam}^{-1}$  in the 0.2-arcsec resolution images. The images also combine high resolution (down to 0.2 arcsec) with high astrometric accuracy ( $< 50$  mas in the HDF) and allow us to probe the association of radio source types with both the optical galaxy population and the sub-mm source population within the HDF and HFF. We note that a comparison of our catalogue with one from WSRT at lower angular resolution suggests that we may be missing  $\sim 10$  per cent of the sources which have low radio surface brightness and angular sizes in the range 5 – 20 arcsec.

Positions derived from the independent MERLIN and VLA imaging agree to better than 15 mas over the entire 10-arcmin field. Radio sources associated with compact galaxies

have been used to align the WFPC2 and CFHT optical fields to the ICRF (Fig. 3 and Table 1). The optical field has been aligned to better than 50 mas in the Deep Field itself, and to  $\sim 150$  mas in the outer parts of the Flanking Fields. The combined optical and radio images are reproduced in Fig. C1.

### 11.2 Interpretation

#### *Radio source characteristics:*

The available radio spectral and morphological data have enabled us to classify 72 per cent of the sources in the 10-arcmin field as either definite or candidate AGNs (20 per cent), or starburst systems (52 per cent). The radio source sizes are typically  $\sim 1$  arcsec (Fig. 4), somewhat smaller than the optical galaxy images. In addition to the imaging of 92 sources found with the VLA alone, the central 3 arcmin, which includes the HDF, has been separately imaged with the MERLIN+VLA combination at the full  $3.3 \mu\text{Jy beam}^{-1}$  sensitivity to search for sources down to  $27 \mu\text{Jy}$ . Although an additional  $\sim 8$  sources are expected to be present from number counts, no additional sources were found that were not previously detected by the VLA, indicating that such sources are heavily resolved with MERLIN and hence must have angular sizes  $\gtrsim 1$  arcsec.

The typical rest-frame luminosity of the AGN and AGN candidate sources is similar to FRI type systems, but is significantly less than that of powerful FRII type radio galaxies and radio-loud quasars. Only two AGN systems show ‘classical’ double radio structures; the vast majority being small core-jet structures extended on sub-galactic scales. All the starburst and starburst candidate sources are substantially more luminous than the nearby starburst galaxy M82, and about half are more luminous than the powerful ULIRG Arp 220. A number of starburst systems at redshifts in excess of 2 have been identified (Chapman et al. 2004a, 2004c submitted) as sub-mm sources with the aid of these radio data and are several orders of magnitude more luminous than Arp 220.

The proportion of starburst systems is found to increase with decreasing source strength (Fig. 7). At flux densities below  $100 \mu\text{Jy}$  more than 70 per cent of the  $\mu\text{Jy}$  sources are starburst-type systems associated with major disc galaxies in the redshift range 0.3–1.3. Some 40 per cent of the brighter sources are found to be intermediate luminosity AGN systems identified with galaxies in a similar redshift range.

#### *Optical identifications:*

We find a *statistical* association of very faint ( $\geq 2 \mu\text{Jy}$ ) radio sources with optically brighter HDF galaxies down to  $\sim 23$  mag (Fig. 5). Of the 92 sources in the 10-arcmin field above  $40 \mu\text{Jy}$ , around 85 per cent are identified with galaxies brighter than  $I = 25$  mag. The remaining 15 per cent are associated with optically faint systems close to or beyond the HFF limit (and for some objects, the HDF limit). As discussed in Section 8.3 many of these may be dust-shrouded starburst galaxies at high redshift ( $z > 3$ ). The high astrometric accuracy of the alignment and the ability of radio to see through obscuring dust have proved to be vital in making the correct optical identification of these very faint radio objects. In particular, this has led to the correct identification

of three optically faint, very red systems (J123642+621331, J123651+621221, and SCUBA HDF850.1). This underscores the vital role to be played by radio observations in probing the distant galaxy population.

#### *X-ray identifications:*

Over half of the radio sources in the 10-arcmin field are detected in X-rays by *Chandra*, however the X-ray detection rate appears to be uncorrelated with the radio source classification or flux density. This does not support the hypothesis that an X-ray detection is a direct diagnostic of AGN activity unless X-ray and radio emission mechanisms have different origins within the same galaxy. This will be investigated further in a later paper.

#### *Sub-mm identifications:*

We have combined our aligned radio and optical fields with the latest sub-mm results on the HDF and HFF. Currently radio observations can provide an important indicator of the correct identification of a high redshift galaxy (eg SCUBA HDF850.1, Dunlop et al. 2004). However, even with the aid of these ultra-sensitive radio observations and excellent radio-optical astrometry, reliable identifications of faint sub-mm sources in the HDF and HFF remain elusive. This will remain the case until sub-arcsecond astrometry in this waveband becomes routinely available with the advent of ALMA.

## ACKNOWLEDGEMENTS

This paper has made use of two radio arrays: MERLIN, a UK National Facility operated by the University of Manchester at Jodrell Bank Observatory on behalf of PPARC, and the VLA of the National Radio Astronomy Observatory a facility of the National Science Foundation operated under cooperative agreement by Associated Universities, Inc. The optical data are based in part on observations made with the NASA/ESA Hubble Space Telescope, obtained at the Space Telescope Science Institute, which is operated by the Association of Universities for Research in Astronomy, Inc., under NASA contract NAS5-26555; and in part on observations made with the Canada-France-Hawaii Telescope by Barger et al. (1999). The cross-matching of the radio source list with the *ISO* (Aussel et al. 1999) and *Chandra* (Alexander et al. 2003) catalogues and other multi-wavelength comparisons made use of software tools developed by the Astronomical Virtual Observatory ([www/euro-vo.org](http://www/euro-vo.org)). We thank the anonymous referee for helpful suggestions.

## REFERENCES

- Alexander D. M., Brandt W. N., Hornschemeier A. E., Garmire G. P., Schneider D. P., Bauer F. E., Griffiths R. E., 2001, *AJ*, 122, 2156
- Alexander D. M., Aussel H., Bauer F. E., et al. 2002, *ApJ*, 568, L85.
- Alexander D. M. et al., 2003, *AJ*, 126, 539
- Aussel H., Cesarsky C. J., Elbaz D., Stark J. L., 1999, *A&A*, 342, 313
- Baars J. W. M., Genzel R., Pauliny-Toth I. I. K., Witzel A., 1977, *A&A*, 61, 99
- Barger A. J., Cowie L. L., Trentham N., Fulton E., Hu E. M., Songaila A., Hall D., 1999, *AJ*, 117, 102
- Barger A. J., Cowie L. L., Brandt W. N., Capak P., Garmire G. P., Hornschemeier A. E., Steffen A. T., Wehner E. H., 2002, *AJ*, 124, 1839
- Bauer F. E. et al., 2002, *AJ*, 123, 1163
- Beasley A. J., Gordon D. G., Fomalont E. B., Peck A., Ma C., Petrov L. 2001, *AAS*, 198.0515B
- Borys C., Chapman S., Halpern M., Scott D., 2003, *MNRAS*, 344, 385
- Carilli C. L., Yun Min S., 1999, *ApJ*, 513, L13
- Carilli C. L., Yun Min S., 2000, *ApJ*, 530, 618
- Chapman S. C., Smail I., Blain A. W., Ivison R. J., 2004a, *ApJ*, 614, 671
- Chapman S. C., Smail I., Windhorst R. A., Muxlow T. W. B., Ivison R. J., 2004b, *ApJ*, 611, 732
- Cohen J. G., Hogg D. W., Blandford R., Cowie L. L., Hu E., Songaila A., Shopbell P., Richberg K., 2000, *ApJ*, 538, 29
- Condon J. J., Yin Q. F., 1990, *ApJ*, 357, 97
- Condon J. J., 1992, *ARA&A*, 30, 575
- Condon J. J., Huang Z. P., Yin Q. F., Thuan T. X., 1991 *ApJ*, 378, 65
- Cowie L. L., Barger A. J., Hu E. M., Capak P., Songaila A., 2004, *ApJ*, 127, 3137
- Cram L. E., Hopkins A., Mobasher B., Rowan-Robinson M., 1998, *ApJ*, 507, 155
- Dawson S., Stern D., Bunker A. J., Spinrad H., Dey A., 2002, *AJ*, 122, 598
- Dickinson M. et al., 2000, *Ap J*, 531, 624
- Dickinson M., 2000, *Philos. Trans. R. Soc. London*, A358 (astro-ph/0004028)
- Dickinson M., et al., 2001 *BAAS*, 198, 2501
- Downes D., et al., 1999, *A&A*, 347, 809
- Dunlop J. S., et al., 2004, *MNRAS*, 350, 769
- Elbaz D., Cesarsky C. J., Chantal P., Aussel H., Franceschini A., Fadda D., Chary R. R., 2002, *A&A*, 384, 848
- Fanaroff B. L., Riley J. M., 1974, *MNRAS*, 167, 31P
- Fomalont E. B., Kellermann K. I., Partridge R. B., Windhorst R. A., Richards E. A., 2002, *AJ*, 123, 2402
- Garrett M. A., 2002, *A&A* 383, L19.
- Garrett M. A., de Bruyn A. G., Giroletti A. G., Baan W. A., Schilizzi R. T., 2000, *A&A*, 361, L41
- Garrett M. A., et al., 2001, *A&A*, 366, L5
- Giavalisco M., et al., 2004, *ApJ*, 600, L93
- Goldschmidt P., et al., 1997, *MNRAS*, 289, 465
- Haiman Z., Dijkstra M., Mesinger, A., 2004, in Merloni A., Nayakshin S., Sunyaev R., eds., "Growing Black Holes", *ESO Astrophysics Symposia*, Springer-Verlag, Berlin.
- Helou G., Soifer B. T., Rowan-Robinson, M., 1985 *ApJ*, 298, 7
- Helou G., Bica 1993, *ApJ*, 415, 93
- Högbom, J. A., 1974, *A&AS*, 15, 417
- Hornschemeier A. E., et al., 2001 *AJ*, 554, 742
- Hughes D. H., et al., 1998, *Nature*, 394, 241
- Ivison R. J., et al., 2002, *MNRAS*, 337, 1
- Lanzetta K. M., Yahil A., Fernandez-Soto A., 1996, *Nature*, 381, 759
- Mann R. G., et al., 1997, *MNRAS*, 289, 482
- Patnaik A. R., Browne I., Wilkinson P. N., Wrobel J., 1992, *MNRAS*, 254, 655
- Phillips A. C., Guzman R., Gallego J., Koo D. C., Lowenthal J. D., Vogt N. P., Faber S. M., Illingworth G. D., 1997, *ApJ*, 489, 543
- Richards E. A., Kellermann K. I., Fomalont E. B., Windhorst R. A., Partidge R. B., 1998, *AJ*, 116, 1039
- Richards, E. A., Fomalont, E. B., Kellermann, K. I., Windhorst, R. A., Partridge, R. B., Cowie, L. L., Barger, A. J., 1999, *ApJ*, 526, 73
- Richards E. A., 2000, *ApJ*, 533, 611

- Rowan-Robinson M., et al., 1997, MNRAS, 289, 490  
T., Laurence, A., Longair, M., Oliver, S., Peacock, J A., 2003,  
Serjeant S., et al., 2003, MNRAS, 344, 887  
Smail I., Ivison R. J., Owen F. N., Blain A. W., Kneib J. P., 2000,  
ApJ, 528, 612  
Strom R. G., 2004, in Bachiller R, Colomer F., Desmurs, J.-F.,  
eds., Proceedings of the 7<sup>th</sup> EVN Symposium, Observatorio  
Astrónomico Nacional, Madrid, p. 271  
Thompson R. J., Storrie-Lombardi L. J., Weymann R. J.,  
Rieke M. J., Schneider G., Stobie E., Lytle D., 1999, AJ,  
117, 17  
Waddington I., Windhorst R. A., Cohen S. H., Partridge R. B.,  
Spinrad H., Stern D., 1999, ApJ, 526, L77  
Williams R. E., et al., 1996, AJ, 112, 1335

**Table A1. Radio Sources in the 10-arcmin Field: Astrometric Characteristics.** The MERLIN+VLA peak position is given unless the source is a VLA-only detection (marked *V*);  $\sigma_{\text{pos}}$  is the error in the position in R. A. and Dec. Beam is the FWHM of the circular restoring beam used for the radio images in Fig. C1. ‘Optical’ refers to the telescope providing the optical image, either C for CFHT (Barger et al. 1999) or H for *HST* WFPC2 (Williams et al. 1996).

Name	MERLIN+VLA Position (Peak)		$\sigma_{\text{pos}}$	Beam	Optical
	R.A.	Dec.	(mas)	( $''$ )	
J123606+620951	12 36 06.6128	+62 09 51.141	4, 5	0.2	–
J123606+621021	12 36 06.8493	+62 10 21.437	39, 29	0.5	–
J123607+621328	12 36 07.1427	+62 13 28.632	34, 62	0.5	–
J123608+621035	12 36 08.1195	+62 10 35.898	4, 4	0.3	C
J123608+621553	12 36 08.2421	+62 15 53.094	47, 45	0.5	C
J123608+621431	12 36 08.9413	+62 14 31.026	78, 38	0.5	C
J123610+620810	12 36 10.5718	+62 08 10.726	14, 15	0.3	–
J123610+621651	12 36 10.5514	+62 16 51.669	38, 30	0.5	C
J123612+621138	12 36 12.0272	+62 11 38.733	80, 108	0.5	C
J123612+621140	12 36 12.4884	+62 11 40.487	49, 47	0.5	C
J123615+620946	12 36 15.6276	+62 09 46.803	71, 53	0.5	C
J123616+621513	12 36 16.1419	+62 15 13.937	51, 53	0.5	C
J123617+621011	12 36 17.0801	+62 10 11.306	32, 28	0.5	C
J123617+621540	12 36 17.5541	+62 15 40.768	5, 5	0.5	C
J123618+621635	12 36 18.017 <i>V</i>	+62 16 35.27 <i>V</i>	56, 41	0.5	C
J123618+621550	12 36 18.3353	+62 15 50.585	4, 4	0.2	C
J123619+621252	12 36 19.4784	+62 12 52.581	13, 11	0.2	C
J123620+620844	12 36 20.2622	+62 08 44.250	3, 3	0.2	C
J123621+621109	12 36 21.2256	+62 11 09.007	29, 27	0.5	C
J123621+621708	12 36 21.2691	+62 17 08.458	5, 5	0.3	C
J123622+621544	12 36 22.4753	+62 15 44.776	41, 49	0.5	H
J123622+621629	12 36 22.6535	+62 16 29.718	78, 69	0.5	C
J123622+620945	12 36 22.7788	+62 09 45.756	63, 53	0.5	C
J123623+621642	12 36 23.5436	+62 16 42.754	1, 1	0.3	C
J123624+621017	12 36 24.2913	+62 10 17.262	53, 38	0.5	H
J123624+621743	12 36 24.7685	+62 17 43.160	22, 27	0.5	C
J123629+621045	12 36 29.1240	+62 10 45.984	7, 50	0.5	C
J123630+620923	12 36 30.0516	+62 09 23.895	46, 52	0.5	C
J123630+620851	12 36 30.4861	+62 08 51.051	69, 62	0.5	C
J123631+620957	12 36 31.2450	+62 09 57.791	8, 10	0.2	H
J123632+621658	12 36 32.412 <i>V</i>	+62 16 58.59 <i>V</i>	140, 140	0.5	C
J123632+620759	12 36 32.5583	+62 07 59.846	18, 25	0.3	–
J123633+621005	12 36 33.7269	+62 10 05.962	67, 63	0.5	H
J123634+621213	12 36 34.4701	+62 12 13.006	16, 22	0.3	H
J123634+621241	12 36 34.5168	+62 12 41.107	11, 11	0.2	H
J123635+621424	12 36 35.5839	+62 14 24.049	7, 7	0.2	H
J123636+621320	12 36 36.9061	+62 13 20.337	35, 28	0.5	H
J123637+620852	12 36 36.9973	+62 08 52.417	36, 26	0.5	C
J123640+621009	12 36 40.6888	+62 10 09.909	43, 40	0.5	H
J123641+620948	12 36 41.5511	+62 09 48.232	14, 16	0.3	H

APPENDIX A: PROPERTIES OF RADIO SOURCES IN THE 10-ARCMIN FIELD

**Table A1** – *continued* **Radio Sources in the 10-arcmin Field: Astrometric Characteristics.**

Name	MERLIN+VLA R.A.	Position (Peak) Dec.	$\sigma_{\text{pos}}$ (mas)	Beam (")	Optical
J123642+621331	12 36 42.0916	+62 13 31.426	1, 1	0.2	H
J123642+621545	12 36 42.2123	+62 15 45.521	11, 12	0.5	C
J123644+621133	12 36 44.3870	+62 11 33.145	1, 1	0.2	H
J123645+620754	12 36 45.862 <i>V</i>	+62 07 54.19 <i>V</i>	89, 68	0.5	–
J123646+621448	12 36 46.0629	+62 14 48.713	5, 4	0.2	C
J123646+621629	12 36 46.3344	+62 16 29.374	19, 19	0.5	C
J123646+621404	12 36 46.3321	+62 14 04.693	2, 2	0.2	H
J123646+620833	12 36 46.6587	+62 08 33.291	49, 49	0.5	C
J123646+621226	12 36 46.673 <i>V</i>	+62 12 26.28 <i>V</i>	190, 190	2.0	H
J123646+621445	12 36 46.736 <i>V</i>	+62 14 45.64 <i>V</i>	70, 68	0.5	H
J123649+621313	12 36 49.7432	+62 13 13.065	42, 30	0.5	H
J123650+620801	12 36 50.1335	+62 08 01.973	19, 19	0.5	–
J123650+620844	12 36 50.1886	+62 08 44.601	37, 35	0.3	C
J123651+621030	12 36 51.1223	+62 10 30.955	29, 32	0.5	H
J123651+621221	12 36 51.7258	+62 12 21.435	34, 18	0.5	H
J123652+621444	12 36 52.8839	+62 14 44.076	6, 6	0.5	H
J123653+621139	12 36 53.3629	+62 11 39.647	14, 10	0.2	H
J123654+621040	12 36 54.6828	+62 10 40.429	38, 53	0.5	H
J123655+620917	12 36 55.7457	+62 09 17.478	16, 23	0.3	C
J123655+620808	12 36 55.9397	+62 08 08.163	10, 13	0.3	–
J123656+621207	12 36 56.5566	+62 12 07.425	41, 34	0.5	H
J123656+621301	12 36 56.9170	+62 13 01.783	97, 75	1.0	H
J123659+621449	12 36 59.9150	+62 14 49.503	68, 86	0.5	H
J123700+620909	12 37 00.2480	+62 09 09.778	1, 1	0.3	C
J123701+621146	12 37 01.5745	+62 11 46.814	38, 78	0.5	H
J123702+621401	12 37 02.759 <i>V</i>	+62 14 01.63 <i>V</i>	40, 40	0.5	H
J123704+620755	12 37 04.1120	+62 07 55.484	64, 91	0.5	–
J123705+621153	12 37 05.8599	+62 11 53.541	79, 83	0.5	H
J123707+621408	12 37 07.2209	+62 14 08.208	60, 49	0.5	C
J123707+621121	12 37 07.9867	+62 11 21.743	28, 33	0.3	C
J123708+621056	12 37 08.3663	+62 10 56.049	20, 21	0.5	H
J123709+620837	12 37 09.4315	+62 08 37.580	6, 6	0.3	C
J123709+620841	12 37 09.7518	+62 08 41.249	16, 11	0.3	C
J123711+621330	12 37 11.2549	+62 13 30.846	12, 14	0.3	C
J123711+621325	12 37 11.9865	+62 13 25.771	32, 38	0.5	C
J123713+621603	12 37 13.5934	+62 16 03.689	90, 87	0.5	C
J123714+621558	12 37 14.3371	+62 15 58.846	52, 77	0.5	C
J123714+620823	12 37 14.9414	+62 08 23.208	1, 1	0.2	C
J123716+621512	12 37 16.3740	+62 15 12.343	2, 2	0.3	C
J123716+621643	12 37 16.5410	+62 16 43.799	31, 51	0.5	C
J123716+621733	12 37 16.6811	+62 17 33.327	2, 2	0.3	C
J123716+621007	12 37 16.8252	+62 10 07.401	19, 22	0.5	C
J123717+620827	12 37 17.520 <i>V</i>	+62 08 27.61 <i>V</i>	51, 91	0.5	C
J123719+620902	12 37 19.9643	+62 09 02.736	62, 43	0.5	C
J123721+621129	12 37 21.2539	+62 11 29.954	1, 1	0.3	H
J123721+621346	12 37 21.4669	+62 13 46.675	58, 54	0.5	C
J123725+620856	12 37 25.0112	+62 08 56.374	24, 26	0.3	C
J123725+621005	12 37 25.298 <i>V</i>	+62 10 05.91 <i>V</i>	98, 60	0.5	C
J123725+621128	12 37 25.9495	+62 11 28.705	2, 2	0.2	C
J123730+621258	12 37 30.7907	+62 12 58.804	4, 5	0.2	–
J123732+621012	12 37 32.644 <i>V</i>	+62 10 12.84 <i>V</i>	180, 180	0.5	–
J123734+620931	12 37 34.242 <i>V</i>	+62 09 31.93 <i>V</i>	140, 140	0.5	–

**Table A2.** Radio Sources in the 10 Arcminute Field – Astrophysical Characteristics

Name	VLA Flux Dens. ( $\mu$ Jy)	LAS (")	WSRT Flux Dens. ( $\mu$ Jy)	Spectral Index	Radio Structure	I or R mag	<i>Chandra</i>	<i>ISO</i>	Radio-Optical Alignment Characteristics	Radio Class	$z$	Ref for $z^1$	WSRT ID
J123606+620951	196	0.9	200/219	>0.56	CE	22.7	Yes	–	Unknown	Uncl	0.6379	CBHCS04	47
J123606+621021	74	0.7	N/A	–	E	23.8	Yes	–	Unknown	SC	2.33	CSWMI04	–
J123607+621328	51	1.2	N/A	–	E	21.8	No	–	Unknown	SC	0.4353	CBHCS04	–
J123608+621035	217	0.6	190/246	0.36	CE	20.6	Yes	–	Central core overlies galaxy nucleus	AGN	0.681	CBHCS04	49
J123608+621553	59	0.5	94/109	–0.24	E	21.0	Yes	–	Source overlies galaxy on edge of CFHT	SC	0.4593	CBHCS04	50
J123608+621431	69	1.0	70/77	–	E	23.7	No	–	Within errors source overlies galaxy	SC	–	–	52
J123610+620810	59	0.6	N/A	–	C1E	–	No	–	Unknown	Uncl	–	–	–
J123610+621651	139	0.9	96/116	–	CE	23.7	No	–	Central component overlies galaxy nucleus	Uncl	–	–	55
J123612+621138	75	1.2	147/147	–	E	18.9	Yes	–	Overlies nuclear region of galaxy	SC	0.275	CBHCS04	58
J123612+621140	102	0.8	with 1138	>0.89	E	19.4	No	–	Overlies nuclear region of galaxy	SC	0.275	CBHCS04	58
J123615+620946	49	0.8	N/A	–	E	22.0	No	–	Overlies nuclear region of galaxy	SC	1.263	CBHCS04	–
J123616+621513	54	1.0	69/69	–	E	22.9	Yes	–	Overlies nuclear region of galaxy	SC	3.61	CSWMI04	62
J123617+621011	62	0.6	96/126	–	CE	21.6	Yes	–	Overlies nuclear region of galaxy	Uncl	0.845	H01	64
J123617+621540	200	1.3	375/543**	>0.55	CE	23.9	No	–	Overlies a faint galaxy in a crowded field	Uncl	1.993	CSBI04	67
J123618+621635	47	2.5	N/A	–	E	19.7	Yes	–	Two sources overlaying merging galaxies ?	AGNC	0.679	H01	–
J123618+621550	151	0.4	with 1540	>0.63	C1E	>25	No	–	Unknown	Uncl	1.87	CSWMI04	67
J123619+621252	108	0.4	117/133	>0.80	E	19.9	Yes	–	Overlies nucleus of a galaxy in a merger	SC	0.473	CBHCS04	69
J123620+620844	123	0.6	115/115	0.01	C1E	21.5	No	–	Central core overlies galaxy nucleus	AGN	1.0178	CBHCS04	71
J123621+621109	53	3.2	83/83	>0.86	E+	21.8	Yes	–	Two sources overlaying merging galaxies ?	SC	1.014	C00	72
J123621+621708	148	2.9	193/193	>0.56	C1E	>25	No	–	Unknown	Uncl	1.993	CSWMI04	73
J123622+621544	84	3.1	N/A	>0.60	E	19.8	Yes	–	Extended emission overlaying galaxy	AGN C	0.6471	CBHCS04	–
J123622+621629	71	1.3	75/143	–	E	23.8	Yes	–	Overlies a faint galaxy in a crowded field	SC	2.40	CSWMI04	74
J123622+620945	51	0.8	61/61	–	E	21.1	No	–	Extended double overlaying galaxy nucleus	SC	0.7479	CBHCS04	75
J123623+621642	481	0.6	476/476	0.63	C1E	23.9	No	–	Overlies a faint galaxy in a crowded field	AGN C	1.918	CSBI04	81
J123624+621017	54	2.1	N/A	–	E	>25	No	–	Unknown	Uncl	–	–	–
J123624+621743	70	0.9	56/108	–	CE	22.9	Yes	–	Overlies nuclear region of galaxy	Uncl	–	–	82
J123629+621045	81	2.7	107/107	>0.86	E	22.2	Yes	–	Extended emission overlaying galaxy	Uncl	1.013	C00	87
J123630+620923	46	0.6	N/A	–	E	22.5	Yes	–	Overlies nuclear region of galaxy	SC	0.953	CBHCS04	–
J123630+620851	48	3.3	74/108	–	E	22.6	No	–	Overlies complex merging galaxy system ?	SC	0.84	CBHCS04	89
J123631+620957	152	0.8	178/180	>0.99	CE	>25	Yes	–	Unknown	Uncl	–	–	90

**Table A2** – *continued* Radio Sources in the 10 Arcminute Field – Astrophysical Characteristics

Name	VLA Flux Dens. ( $\mu$ Jy)	LAS (")	WSRT Flux Dens. ( $\mu$ Jy)	Spectral Index	Radio Structure	I or R mag	<i>Chandra</i>	<i>ISO</i>	Radio-Optical Alignment Characteristics	Radio Class	$z$	Ref for $z^1$	WSRT ID
J123632+621658	82	4.0	97/122	–	E+	18.2	No	–	Overlies face of galaxy	SC	0.437	CBHCS04	92
J123632+620759	91	2.6	91/91	>0.58	CE+	24.0	Yes	–	Unknown	Uncl	1.9939	CBHCS04	93
J123633+621005	46	1.2	N/A	>0.98	E	21.6	Yes	No	Overlies nuclear region of face-on spiral	SC	1.016	CBHCS04	–
J123634+621213	233	1.2	244/253	0.74	CE	18.7	Yes	Yes	Overlies nucleus of galaxy with a dust lane	S	0.456	CBHCS04	96
J123634+621241	230	1.0	187/187	0.74	CE	22.3	Yes	Yes	Overlies nuclear region of galaxy	S	1.219	C00	95
J123635+621424	88	0.3	102/121	>0.87	C	22.6	Yes	Yes	Overlies bright nucleus of face-on spiral	S*	2.011	D02	99
J123636+621320	50	0.7	N/A	–	E	>25	Yes	No	Unknown	SC	–	–	–
J123637+620852	71	1.1	78/78	>0.82	E	24.5	No	–	Overlies a faint galaxy in a crowded field	SC	–	–	101
J123640+621009	87	1.2	120/122	0.44	E	23.9	No	No	Northerly component overlies faint galaxy	AGN C	1.958	CSBI04	107
J123641+620948	76	0.6	108/191	>0.56	CE	20.2	Yes	–	Overlies nucleus of (merging ?) disc galaxy	Uncl	0.518	C00	109
J123642+621331	467	0.4	489/489	0.94	C1E	>25	Yes	Yes	Overlies very red NICMOS detection	S*	4.424	W99	111
J123642+621545	150	1.7	88/89	0.50	CE	20.7	Yes	Yes	Overlies nuclear region of galaxy	Uncl	0.857	H01	110
J123644+621133	1290	12.0	1190/1606	0.30	FR1	20.9	Yes	Yes	Core overlies nucleus of elliptical galaxy	AGN	1.050	C00	113
J123645+620754	49	3.0	67/67	–	E	23.0	Yes	–	Unknown	Uncl	1.433	CBHCS04	114
J123646+621448	124	0.5	186/262**	0.84	C1E	25.5	Yes	No	Overlies nucleus of faint red galaxy	Uncl	(1.7)	CSWMI04	118
J123646+621629	393	2.4	422/422	>1.62	CE	19.8	No	–	Overlies nuclear region of galaxy	SC	0.502	C00	116
J123646+621404	179	0.5	187/187	–0.04	C1E	20.7	Yes	Yes	Core overlies nucleus of galaxy	AGN	0.961	CBHCS04	115
J123646+620833	80	0.8	130/155	>0.61	E	20.6	Yes	–	Overlies nuclear region of galaxy	SC	0.9712	CBHCS04	119
J123646+621226	72	3.2	N/A	>1.14	E	>28	No	No	Unknown	Uncl	–	–	–
J123646+621445	117	2.3	with 1448	0.98	E	23.9	Yes	No	Straddles a faint compact galaxy	Uncl	–	–	118
J123649+621313	49	1.0	68/68	0.72	E	21.1	Yes	Yes	Overlies nuclear region of galaxy	S	0.475	C00	123
J123650+620801	54	0.7	N/A	–	E	22.2	No	–	Unknown	SC	0.559	CBHCS04	–
J123650+620844	76	0.8	84/116	>0.80	CE	20.0	No	–	Overlies nuclear region of galaxy	SC	0.434	CBHCS04	124
J123651+621030	95	1.2	69/71	0.74	E	19.9	Yes	Yes	Overlies nuclear region of galaxy	S	0.410	C00	126
J123651+621221	49	1.2	57/57	0.71	E	>28	Yes	Yes	Overlies faint red emission at I 29 mag	S*	(2.7)	H01	131
J123652+621444	168	1.3	237/276	–0.12	C1E	18.5	Yes	No	Core overlies nucleus of elliptical galaxy	AGN	0.321	CBHCS04	133
J123653+621139	66	0.3	73/73	0.77	C1E	21.9	Yes	Yes	Overlies nuclear region of compact galaxy	S	1.275	C00	134
J123654+621040	48	1.5	N/A	>1.00	E+	>25	No	No	Unknown	SC	–	–	–
J123655+620917	64	0.6	88/88	>0.55	CE	20.4	No	–	Overlies nuclear region of galaxy	Uncl	0.419	CBHCS04	138
J123655+620808	106	0.7	128/129	>0.85	CE	22.6	Yes	–	Unknown	Uncl	0.792	CBHCS04	137



**Table A2** – *continued* Radio Sources in the 10 Arcminute Field – Astrophysical Characteristics

Name	VLA Flux Dens. ( $\mu$ Jy)	LAS (")	WSRT Flux Dens. ( $\mu$ Jy)	Spectral Index	Radio Structure	I or R mag	<i>Chandra</i>	<i>ISO</i>	Radio-Optical Alignment Characteristics	Radio Class	$z$	Ref for $z^1$	WSRT ID
J123656+621207	46	1.0	N/A	>1.32	E	>25	No	No	Unknown	SC	–		–
J123656+621301	49	1.2	N/A	>1.22	E	22.5	Yes	Yes	Overlies compact galaxy in crowded field	S	0.474	C00	–
J123659+621449	47	1.0	N/A	–	E	20.9	Yes	Yes	Overlies nucleus of a galaxy in a merger ?	SC	0.761	CBHCS04	–
J123700+620909	324	0.4	236/236	0.89	C1E	>25	No	–	Unknown	AGN C	–		142
J123701+621146	128	3.0	110/122	0.67	E+	>25	Yes	Yes	Unknown	S	(1.52)	BCB+02	143
J123702+621401	41	3.4	54/54	>0.79	E+	21.9	No	Yes	SE component overlies galaxy	Uncl	1.2463	CBHCS04	145
J123704+620755	51	1.0	N/A	–	E	–	Yes	–	Unknown	SC	1.253	BCB+02	–
J123705+621153	52	1.5	N/A	>1.27	E	20.6	Yes	Yes	Overlies nuclear region of face-on spiral	S	0.902	CBHCS04	–
J123707+621408	45	0.9	N/A	0.29	E	24.9	Yes	No	Overlies nuclear region of faint galaxy	SC	2.48	CSWMI04	–
J123707+621121	60	0.6	66/83	>0.82	E	25	No	No	Overlies faint galaxy	SC	–		153
J123708+621056	45	0.7	125/125	0.35	E	19.8	Yes	No	Overlies central region of edge-on disc galaxy	SC	0.422	CBHCS04	155
J123709+620837	72	0.5	310/357	–0.35	CE	20.4	Yes	–	Core overlies nucleus of galaxy	AGN	0.907	CBHCS04	156
J123709+620841	68	0.8	with 0837	–	CE	21.4	Yes	–	Core overlies nucleus of galaxy	AGN C	0.902	CBHCS04	156
J123711+621330	132	1.2	172/179	0.69	C1E	22.7	Yes	–	Overlies brightest region of asymmetrical galaxy	AGN C	(1.112)	B02	157
J123711+621325	54	0.8	with 1331	>1.16	E	25.0	Yes	–	Overlies faint galaxy	SC	1.99	CSWMI04	157
J123713+621603	55	0.9	57/57	–	E	22.8	No	–	Overlies nuclear region of galaxy	SC	0.9375	CBHCS04	161
J123714+621558	51	1.5	N/A	–	E	20.8	No	–	Overlies central region of galaxy	SC	0.567	C00	–
J123714+620823	1350	0.05	1853/1853	–0.15	C	22.0	No	–	Core overlies nuclear region of galaxy	AGN	–		163
J123716+621512	187	0.4	166/166	0.41	C1E	19.8	Yes	–	Core overlies nuclear region of galaxy	AGN C	0.230	CBHCS04	165
J123716+621643	66	0.9	81/81	–	E	21.6	Yes	–	Overlies region between merging galaxies	SC	0.557	C00	168
J123716+621733	346	0.6	362/362	>0.76	C1E	22.2	Yes	–	Core overlies nuclear region of galaxy	AGN C	1.146	CBHCS04	166
J123716+621007	63	0.7	92/92	–	E	19.9	Yes	–	Overlies nuclear region of galaxy	SC	0.411	C00	167
J123717+620827	126	2.1	with 1733	>0.77	E+	19.7	No	–	Overlies nuclear region of merging galaxy ?	SC	–		166
J123719+620902	51	0.7	N/A	–	E	22.1	No	–	Overlies nucleus of galaxy in crowded field	SC	–		–
J123721+621129	383	0.8	381/381	–0.28	C1E	>25	Yes	–	Unknown	AGN	1.56	BCB+02	172
J123721+621346	50	0.7	67/68	>0.66	E	22.1	No	–	Overlies nuclear region of galaxy	SC	1.019	C00	171
J123725+620856	90	0.4	90/90	–	C1E	22.1	Yes	–	Overlies nuclear region of galaxy	Uncl	(0.984)	B02	178
J123725+621005	117	3.8	109/109	–	E	19.1	No	–	Straddles central region of galaxy	Uncl	(0.360)	B02	179
J123725+621128	5960	3.8	5291/5316	1.35	WAT	22.9	No	–	Core overlies nucleus of compact galaxy	AGN	–		182
J123730+621258	107	0.3	140/140	>0.79	CE	–	No	–	Unknown	Uncl	–		187
J123732+621012	51	1.9	82/82	–	E	–	No	–	Unknown	Uncl	–		190
J123734+620931	142	2.8	137/161	–	E	–	Yes	–	Unknown	Uncl	0.189	BCB+02	193

**Table A2** – *continued* Radio Sources in the 10 Arcminute Field – Astrophysical Characteristics:<sup>1</sup>References for redshifts  $z$ 

BCB+02	Barger et al. (2002)
B02	Bauer et al. (2002)
CSBI04	Chapman et al.(2004a) (received after submission; data not included in figures.)
CSWMI04	Chapman et al.(2004b) (received after submission; data not included in figures.)
C00	Cohen et al. (2000)
CBHCS04	Cowie et al. (2004); Team Keck Redshift Survey <a href="http://www2.keck.hawaii.edu/realpublic/science/tksurvey/index.html">http://www2.keck.hawaii.edu/realpublic/science/tksurvey/index.html</a>
D02	Dawson et al. (2002)
H01	Hornschemeier et al. (2001)
W99	Waddington et al. (1999)

## APPENDIX B: SOURCE DETAILS FOR THE 10-ARCMINUTE FIELD

In this section we give a brief description of the properties of each source detected and imaged in the 10-arcmin field. Where known, radio spectral indices are given ( $S \propto \nu^{-\alpha}$ ). For weaker sources close to the edge of the 10-arcmin field, spectral index information is unavailable since they are on the edge of the VLA primary beam response at 8.4 GHz and are thus undetected by Richards et al. (1998). For stronger sources in this region, which still remain undetected at 8.4 GHz, lower limits to the radio spectral index are given. We note other detections and compare the radio and optical morphologies; however we cannot assume that the emission at different wavelengths comes from the same part of the galaxy or the same mechanism unless there is additional evidence for this, including the tight radio-far-IR correlation (see references in Section 8.2). Table A2 gives additional information (such as whether non-detections at other wavelengths are due to the limited fields of view of the relevant instruments). *ISO* data are taken from Aussel et al. (1999) and *Chandra* data are taken from Hornschemeier et al. (2001) and Alexander et al. (2003). We have not yet included the latest *HST* ACS data for reasons noted in Section 10.

**J123606+620951** (Unclassified): is undetected at 8.4 GHz and thus has a radio spectrum with  $\alpha > 0.56$ . It has a compact ( $<0.2$  arcsec) component with weak extended emission. The radio source lies outside the CFHT image so no optical frame is shown in Fig. C1. However Cowie et al. (2004) catalogue an  $R = 22.7$  mag galaxy at the position of the radio source with a redshift of 0.6379. It is detected by *Chandra*.

**J123606+621021** (Starburst Candidate): is separated from J123608+621035 by 17 arcsec but does not appear to be related to it. The radio structure is extended over 0.7 arcsec. It lies outside the area of the CFHT image so no optical frame is shown in Fig. C1. However Chapman et al. (2004b) catalogue an  $I=23.8$  mag sub-mm galaxy ( $S_{850} = 11.6 \pm 3.5$  mJy) at the position of the radio source with a redshift of 2.33. There is a faint *Chandra* counterpart.

**J123607+621328** (Starburst Candidate): is extended over 1.2 arcsec roughly NS. This source lies outside the CFHT image so no optical frame is shown in Fig. C1. However Cowie et al. (2004) catalogue an  $R = 21.8$  mag galaxy at the position of the radio source with a redshift of 0.4353.

**J123608+621035** (AGN): has a relatively flat radio spectrum overall ( $\alpha=0.36$ ). It has a compact core and two-sided radio emission. The compact component lies at the nucleus of a 20.6 mag galaxy with a redshift of 0.681 (Cowie et al. 2004). It is detected by *Chandra*.

**J123608+621553** (Starburst Candidate): Richards (2000) states that this source has an inverted radio spectrum ( $\alpha = -0.24$ ). It is extended by approximately 0.5 arcsec. It is identified with a  $I = 21$  mag galaxy at the very edge of the CFHT frame with a redshift of 0.4593 (Cowie et al. 2004). No compact AGN core is seen, therefore it is most likely that the radio emission originates in an extended starburst with strong free-free absorption at 1.4 GHz to account for the spectral shape. It is detected by *Chandra*.

**J123608+621431** (Starburst Candidate): is extended by  $\sim 1$  arcsec EW and is identified with a 23.7 mag galaxy of the CFHT frame.

**J123610+620810** (Unclassified): has a relatively compact component with weak extended emission  $\sim 0.6$  arcsec to the SW at 0.5-arcsec resolution (not shown). No optical information is available since it lies outside the area of the CFHT frame.

**J123610+621651** (Unclassified): has extended radio emission (0.9 arcsec) on both sides of a relatively compact component at 0.2-arcsec resolution (not shown), which is coincident with the nuclear region of a  $I = 23.7$  mag galaxy.

**J123612+621138/J123612+621140** (Starburst Candidates): are separated by  $\sim 4$  arcsec. J123612+621140 has a steep radio spectrum ( $\alpha > 0.89$ ). J123612+621138 has no spectral index measurement although the radio sources are only partially separated by Richards (2000) who classifies the pair as a single object. Each one appears to be an extended starburst and is identified with a separate galaxy in a system which appears to be interacting. J123612+621138 is identified with an  $I = 18.9$  mag galaxy; J123612+621140 is identified with an  $I = 19.4$  mag galaxy. Cowie et al. (2004) measure the same redshift for each galaxy ( $z = 0.275$ ). J123612+621138 is detected by *Chandra*.

**J123615+620946** (Starburst Candidate): is extended over  $\sim 0.8$  arcsec and overlies the nuclear region of an  $I = 22.0$  mag galaxy with a redshift of 1.263 (Cowie et al. 2004).

**J123616+621513** (Starburst Candidate): is extended over  $\sim 1$  arcsec. The weak extended emission  $\sim 3$  arcsec to the NW is only visible at low resolution and has no optical counterpart. It is not thought to be associated with J123616+621513 and falls below the  $7\sigma$  detection threshold for the 10-arcmin field sample. J123616+621513 is identified with an  $I = 22.9$  mag galaxy. Chapman et al. (2004b) identify the system as a sub-mm galaxy ( $S_{850} = 5.8 \pm 1.1$  mJy) with a redshift of 3.61. It is detected by *Chandra*.

**J123617+621011** (Unclassified): is extended over  $\sim 0.6$  arcsec and contains a compact component at 0.2-arcsec resolution (not shown). The nature of the object is unclear since the radio structure could originate from AGN or starburst activity (or both). It is identified with a  $I = 21.6$  mag galaxy. Hornschemeier et al. (2001) find a single emission line at 6879.3 Å which they assign as [OII] at a redshift of 0.845. It is detected by *Chandra* with a X-ray luminosity strongly suggestive of AGN activity.

**J123617+621540** (Unclassified): has a fairly steep radio spectrum ( $\alpha > 0.55$ ). It contains a compact component with two-sided emission extended over 1.3 arcsec. It is identified with a faint galaxy ( $I = 23.9$  mag) in a complex region on the CFHT frame.

**J123618+621635** (AGN Candidate): contains two extended radio components separated by 2.5 arcsec. The radio component to the SE overlies the central region of an  $I = 19.7$  mag galaxy and shows no evidence for any compact core. The NW radio component appears to be associated with a second galaxy which may be part of an interacting system. Hornschemeier et al. (2001) find two emission lines from the SE component which they assign to be [OIII] at a redshift of 0.679. It is also detected by *Chandra*. On the basis of the X-ray luminosity and a weak [NeV] feature, Hornschemeier et al. (2001) suggest that this object is an AGN system.

**J123618+621550** (Unclassified): exhibits a steep radio spectrum ( $\alpha > 0.63$ ) compact component with one-sided

emission extended over 0.4 arcsec. It is unidentified at the limit of the CFHT frame. Chapman et al. (2004b) identify the system as a possible sub-mm galaxy ( $S_{850} = 7.3 \pm 1.1$  mJy) with a redshift of 1.87. However, this identification is uncertain since the measured redshift is for the optical object approximately 0.5 arcsec to the SW of the radio source; this is above the nominal astrometric alignment errors for the position of the radio source in the 10-arcmin field.

**J123619+621252** (Starburst Candidate): has a steep radio spectrum ( $\alpha > 0.8$ ) and has radio emission extended over 0.4 arcsec. It lies at the nucleus of an  $I = 19.9$  mag galaxy at redshift = 0.473 (Cowie et al. 2004). The optical galaxy appears to have a companion and may be part of a merging system. It is detected by *Chandra*.

**J123620+620844** (AGN): has a flat radio spectrum ( $\alpha = 0.01$ ) and shows a compact core with a one-sided (0.6 arcsec) extension to the east. The core component overlies the nucleus of an  $I = 21.5$  mag galaxy at a redshift of 1.0178 (Cowie et al. 2004).

**J123621+621109** (Starburst Candidate): has a steep radio spectrum ( $\alpha > 0.86$ ). The VLA-only image (not shown) reveals additional low surface brightness emission extending over 3 arcsec to the north-east. A brighter but still extended component is seen in the combination image and overlies the fainter, south-western member of an  $I = 21.8$  mag pair of merging galaxies at a redshift of 1.014 (Cohen et al. 2000). There is a *Chandra* counterpart.

**J123621+621708** (Unclassified): has a steep radio spectrum ( $\alpha > 0.56$ ) and contains a compact component with one-sided emission extending to the south-east. An extended radio component lies 2.5 arcsec to the north-west, close to the position of an  $I = 23.4$  mag galaxy on the CFHT frame. There is no optical object brighter than  $I = 25$  mag at the position of the compact radio component. Chapman et al. (2004b) identify the system as a possible sub-mm galaxy ( $S_{850} = 7.8 \pm 1.9$  mJy) with a redshift of 1.99. However, this identification is uncertain since the measured redshift is for the galaxy to the NW of the radio source; this is well above the nominal astrometric alignment errors for the position of the radio source in the 10-arcmin field.

**J123622+621544** (AGN Candidate): has a steep radio spectrum ( $\alpha > 0.6$ ). The radio structure is extended and low surface-brightness emission seen in the VLA-only image (not shown) extends for nearly 3 arcsec to the north-west. A brighter region of emission region lies 0.75 arcsec to the south-east of the bright nucleus of an  $I = 19.8$  mag spiral galaxy in the HFF at a redshift of 0.6471 (Cowie et al. 2004). As the radio emission extends well beyond the optical galaxy the source is classified as an AGN candidate with an undetected core. There is a faint *Chandra* counterpart.

**J123622+621629** (Starburst Candidate): is extended (1.3 arcsec) and is identified with an  $I = 23.8$  mag galaxy on the CFHT frame. Chapman et al. (2004b) identify the system as a sub-mm galaxy ( $S_{850} = 7.7 \pm 1.3$  mJy) with a redshift of 2.40. There is a faint *Chandra* counterpart

**J123622+620945** (Starburst Candidate): is extended over  $\sim 0.8$  arcsec and shows evidence for double structure at position angle 110 degrees. There is no evidence of any compact radio structure at full resolution. The source overlies the nuclear region of an  $I = 21.1$  mag galaxy with a redshift of 0.7479 (Cowie et al. 2004).

**J123623+621642** (AGN Candidate): has a steep radio spectrum ( $\alpha = 0.63$ ) and contains a compact component together with one-sided extended emission. It is identified with an  $I = 23.9$  mag galaxy in a complex region on the CFHT frame.

**J123624+621017** (Unclassified): consists of two extended components separated by 2.1 arcsec at position angle  $30^\circ$ . Each component is  $\sim 0.5$  arcsec in size and there is no evidence for any compact radio structure at 0.2-arcsec resolution. The source cannot be identified with any optical object brighter than  $I = 25$  mag in the HFF frame.

**J123624+621743** (Unclassified): shows a compact feature in the 0.2 arcsec image (not shown) with additional emission extending over 0.9 arcsec. It is identified with a  $I = 22.9$  mag galaxy and has a faint *Chandra* counterpart.

**J123629+621045** (Unclassified): has a steep radio spectrum with  $\alpha > 0.86$  and is extended east-west over 2.7 arcsec with no evidence of compact emission at the highest angular resolution. The eastern end of the radio source is coincident with the nucleus of an  $I = 22.2$  mag galaxy at a redshift of 1.013 on the CFHT frame (Cohen et al. 2000) but the extension is not correlated with optical emission. Chapman et al. (2004b) identify this system as a sub-mm source ( $S_{850} = 5.0 \pm 1.3$  mJy). It is detected by *Chandra*.

**J123630+620923** (Starburst Candidate): is extended over 0.6 arcsec and overlies the nuclear region of an  $I = 22.5$  mag galaxy on the CFHT frame with an estimated photometric redshift of 0.953 (Bauer et al. 2002). It is detected by *Chandra*.

**J123630+620851** (Starburst Candidate): is extended over 3.3 arcsec. The extension is more clearly seen in the VLA-only image (not shown) and additional flux is seen with the Westerbork radio telescope indicating possible emission on the 10-arcsec scale. The radio structure roughly follows the optical isophotes of a complex galaxy system that appears to be interacting, the brightest member of which has  $I = 22.6$  mag.

**J123631+620957** (Unclassified): has a steep radio spectrum ( $\alpha > 0.99$ ) and a compact component with two-sided emission extending over 0.8 arcsec. There is no optical counterpart brighter than  $I = 25$  mag on the HFF frame but it has a faint *Chandra* counterpart.

**J123632+621658** (Starburst Candidate): is extended over  $\sim 4$  arcsec on the VLA-only image (not shown) and shows no sign of compact emission at higher resolution. The source is very heavily resolved with MERLIN and the position in Table A1 is taken from the VLA-only image at 2-arcsec resolution. The source is associated with an  $I = 18.2$  mag spiral galaxy with a redshift of 0.437 (Cowie et al. 2004).

**J123632+620759** (Unclassified): has a steep radio spectrum ( $\alpha > 0.58$ ) and is extended over some 2.6 arcsec on the VLA-only image (not shown). At higher resolution a compact component is found with two-sided extended emission, although the majority of the extended emission seen in the VLA-only image is resolved out. The radio source lies outside the CFHT frame so no optical image is shown in Fig. C1. However Cowie et al. (2004) catalogue an  $R = 24.0$  mag galaxy at the position of the radio source with a redshift of 1.9939. It is detected by *Chandra*.

**J123633+621005** (Starburst Candidate): has a steep radio spectrum ( $\alpha > 0.98$ ) and is extended over approximately 1.2 arcsec. There is no evidence for any compact

emission at the highest angular resolution. It overlies a face-on  $I = 21.6$  mag spiral galaxy at a redshift of 1.016 (Cowie et al. 2004) on the HFF frame. It is detected by *Chandra*.

**J123634+621213** (Starburst): has a steep radio spectrum ( $\alpha = 0.74$ ). The extended radio emission is two-sided, surrounding a compact component. However EVN observations at 20 mas resolution do not detect this compact component (Garrett et al. 2001). The source is identified with a bright disc galaxy ( $I = 18.7$  mag), at a redshift of 0.456 (Cowie et al. 2004). The HFF optical image shows evidence for a dust-lane or possible double nucleus which may indicate a recent merger. The brightest radio emission lies between the optical nuclei and the extensions follow the optical isophotal ridge-line. The galaxy is also detected by *ISO* with  $S_{15\mu\text{m}} = 448 \mu\text{Jy}$ . X-ray emission is detected by *Chandra*.

**J123634+621241** (Starburst): has a steep radio spectrum ( $\alpha = 0.74$ ). There is extended emission to the south-west of a compact component which is not detected by the EVN at 20 mas resolution (Garrett et al. 2001). The compact component overlies the nuclear region of an  $I = 22.3$  mag Scd galaxy at a redshift of 1.219 on the HFF WFPC2 frame (Cohen et al. 2000). It has an mid-IR flux density  $S_{15\mu\text{m}} = 363 \mu\text{Jy}$  as detected by *ISO*, which implies a substantial star-formation rate. This source is the most likely radio counterpart to SCUBA HDF850.7 (see Section 8.4.1). There is a faint *Chandra* counterpart.

**J123635+621424** (Starburst + AGN?): has a steep radio spectrum ( $\alpha > 0.87$ ). It appears relatively compact, with an angular size of only  $\leq 0.3$  arcsec, in contrast to the earlier angular size estimate of 2.8 arcsec reported by Richards et al. (1998). The radio source overlies the bright optical nucleus of a face-on  $I = 22.6$  mag spiral galaxy on the HFF frame. The spatial extent of the galaxy suggests that it is of low to moderate redshift. However, Bauer et al. (2002) list this object as having a spectroscopic redshift close to 2 and Dawson et al. (2002) assign a redshift of 2.011 from several detected emission lines. It is an *ISO* detection and Chapman et al. (2004b) identify the system as a sub-mm galaxy ( $S_{850} = 5.5 \pm 1.4$  mJy) at a redshift of 2.01. It is detected by *Chandra*. Dawson et al. (2002) argue that the 15  $\mu\text{m}$  and X-ray detections are indicative of an AGN system. If this object is a compact nuclear starburst system, the implied star-formation rate from the radio and IR flux densities is very large ( $\sim 1800 M_{\odot} \text{ yr}^{-1}$ ).

**J123636+621320** (Starburst Candidate): is extended over approximately 0.7 arcsec and shows no sign of compact emission. There is no optical counterpart brighter than  $I = 25$  mag at the radio source position on the HFF frame. There is a faint *Chandra* counterpart.

**J123637+620852** (Starburst Candidate): has a steep radio spectrum ( $\alpha > 0.82$ ), is extended east-west over approximately 1.1 arcsec and shows no sign of a compact component. It is identified with an  $I = 24.5$  mag galaxy in a complex region on the CFHT frame.

**J123640+621009** (AGN Candidate): consists of two components separated by 1.2 arcsec. The source as a whole has a radio spectrum of  $\alpha = 0.44$ , which suggests the presence of a flat-spectrum component. The 8.4-GHz position (Richards et al. 1998) is close to the northerly component indicating that it has a flat spectrum and therefore may be associated with an AGN. Although no evidence for a compact feature can be found at 1.4 GHz, the radio image has

a low signal-to-noise ratio. The more northerly component overlies a faint compact  $I = 23.9$  mag galaxy on the HFF frame.

**J123641+620948** (Unclassified): has a steep radio spectrum ( $\alpha > 0.56$ ) and contains a compact radio component with some extended emission with a total angular extent of approximately 0.6 arcsec. The compact component coincides with the nucleus of an  $I = 20.2$  mag disc galaxy at a redshift of 0.518 which may be part of a merging system (Cohen et al. 2000). The extended radio emission lies perpendicular to the major axis of the optical galaxy. There is a faint *Chandra* counterpart.

**J123642+621331** (Starburst + AGN?): has a steep radio spectrum ( $\alpha = 0.94$ ). The radio structure consists of a compact component together with emission extended over 0.4 arcsec. Garrett et al. (2001) detect the dominant compact component with the EVN at an angular resolution of 20 mas; it may therefore be a steep-spectrum AGN core. There is no optical counterpart at the detection threshold in the HFF  $I$ -band image. Waddington et al. (1999) detect a very red object at the radio source position with NICMOS, in J and H-band, and with the KPNO 4-m in  $K$ -band. On the basis of a single Ly $\alpha$  emission line and the observed spectral energy distribution, they ascribe a redshift of 4.424 and argue that it is a distant starburst galaxy with a weak embedded AGN. This interpretation is consistent with the radio morphology. The source is detected by both *ISO* and *Chandra*.

**J123642+621545** (Unclassified): has an intermediate radio spectrum ( $\alpha = 0.50$ ). The radio structure consists of a compact component and extended emission to the NE and SW with the latter reaching nearly 1.5 arcseconds from the core. The core component overlies the nucleus of an  $I = 20.7$  mag galaxy on the CFHT frame at a redshift of 0.857 (Hornschemeier et al. 2001). The source is detected by both *ISO* and *Chandra*; the compact component could be an AGN, but the nature of this object remains unclear.

**J123644+621133** (AGN – FRI radio galaxy): has a bright core with a flat radio spectrum ( $\alpha = 0.1$ , Richards et al. 1998) with steep spectrum emission oriented N–S and extending for about 15 arcsec in the VLA-only image (not shown). Overall the radio source exhibits a classical FRI structure. It is optically identified with an  $I = 20.9$  mag elliptical galaxy at a redshift of 1.050 (Cohen et al. 2000). This source is not catalogued by Aussel et al. (1999) but Goldschmidt et al. (1997) list a nearby *ISO* detection at 6.7  $\mu\text{m}$  only; Mann et al. (1997) identify this with the host of J123644+621133. There is a faint *Chandra* counterpart.

**J123645+620754** (Unclassified): lies close to the edge of the 10-arcmin field. The source is extended east-west over some 3 arcsec, and there is no evidence for any compact emission. The position given in Table A1 is from the VLA-only image at 2-arcsec resolution. The radio source lies outside the CFHT frame so no optical image is shown in Fig. C1. However Cowie et al. (2004) catalogue an  $R = 23.0$  mag galaxy at the position of the radio source with a redshift of 1.433. There is a faint *Chandra* counterpart.

**J123646+621448** (Unclassified): has a steep radio spectrum, ( $\alpha > 0.84$ ) and contains a compact component with a one-sided 0.5 arcsec extension at a position angle of  $\approx 160$  degrees. It is not identified on the HFF frame to approximately  $I = 25$  mag. However, on the lower resolution

CFHT frame it overlies a faint but distinct galaxy ( $I = 25.5$  mag). Chapman et al. (2004b) identify this system as a sub-mm source ( $S_{850} = 10.3 \pm 2.2$  mJy). There is a faint *Chandra* counterpart.

**J123646+621629** (Starburst Candidate): has a very steep radio spectrum ( $\alpha > 1.62$ ). The radio structure consists of a compact central feature together with extended emission distributed symmetrically around it with a total angular extent of about 2.4 arcsec. The radio core is coincident with the nuclear region of an  $I = 19.8$  mag galaxy at a redshift of 0.502 (Cohen et al. 2000).

**J123646+621404** (AGN): has an inverted radio spectrum ( $\alpha = -0.04$ ). The radio structure has a compact component and two-sided extended emission. The radio emission overlies the nucleus of a nearly face-on disc galaxy ( $I = 20.7$  mag) at a redshift of 0.961 (Cowie et al. 2004), which exhibits a broad emission line spectrum (Phillips et al. 1997). These observations combine to form strong evidence that this galaxy contains an AGN. This radio source was detected by *ISO* with  $S_{7\mu\text{m}} = 52 \mu\text{Jy}$  and it has a bright *Chandra* counterpart. Although Rowan-Robinson et al. (1997) interpret this source as a massive starburst, star-formation seems unlikely to be powering the bulk of the radio emission in this object.

**J123646+620833** (Starburst Candidate): has a steep radio spectrum ( $\alpha > 0.61$ ). The radio structure is extended over 0.8 arcsec and shows no sign of compact emission at 0.2-arcsec resolution. The radio emission overlies the nuclear region of an  $I = 20.6$  mag galaxy at a redshift of 0.9712 (Cowie et al. 2004). There is a faint *Chandra* counterpart.

**J123646+621226** (Unclassified): has a steep radio spectrum ( $\alpha > 1.14$ ) and is completely resolved-out at 0.2-arcsec resolution. The VLA-only image (as shown in Fig. C2) shows the source to be 3.2 arcsec in extent. No optical counterpart brighter than  $I = 28$  mag is found at the radio position. Deep near-infrared observations (Thompson et al. 1999) place magnitude limits of  $I_{\text{AB}} > 28.5$ ,  $J_{110} > 29$ , and  $H_{160} > 29$  mag.

**J123646+621445** (Unclassified): has a steep radio spectrum ( $\alpha = 0.98$ ) and is extended over 2.3 arcsec with the major axis roughly aligned with J123646+621448 which lies 6 arcsec to the north west. However, J123646+621445 overlies a fairly compact faint ( $I \sim 23.9$  mag) galaxy. Since both sources overlie separate optical identifications, it is most likely that they are unrelated. The  $I = 20.4$  mag galaxy 2.5 arcsec to the NE of J123646+621445 has a measured redshift of 0.558 (Cohen et al. 2000), but does not seem to be related to the radio source. The *ISO* source at 4 arcsec separation in a similar direction cannot therefore be identified with the radio source with any confidence.

**J123649+621313** (Starburst): has a steep radio spectrum ( $\alpha = 0.72$ ) with no evidence of any compact structure at 0.2-arcsec resolution. It is extended by approximately 1 arcsec along the major axis of an  $I = 21.1$  mag disc galaxy at a redshift of 0.475 (Cohen et al. 2000). The galaxy is in the *ISO* catalog of HDF sources with  $S_{15\mu\text{m}} = 320 \mu\text{Jy}$  and may be associated with SCUBA HDF850.4 (see Section 8.4.3). There is a faint *Chandra* counterpart. Low level radio emission below the formal detection threshold (and hence not in the catalogue) may also be seen from an  $I = 22.7$  mag disc galaxy located about 3 arcsec to the north which lies at a redshift of 1.238 (Cohen et al. 2000).

**J123650+620801** (Starburst Candidate): is extended by approximately 0.7 arcsec and shows no sign of compact structure at 0.2-arcsec resolution. The radio source lies outside the CFHT image so no optical frame is shown in Fig. C1. However Cowie et al. (2004) catalogue an  $R = 22.2$  mag galaxy at the position of the radio source with a redshift of 0.559.

**J123650+620844** (Starburst Candidate): has a steep spectrum ( $\alpha > 0.80$ ). The radio structure shows a compact component together with extended emission of approximately 0.8 arcsec extent. The compact component overlies the nucleus of an  $I = 20.0$  mag galaxy at a redshift of 0.434 (Cowie et al. 2004).

**J123651+621030** (Starburst): has a steep-spectrum ( $\alpha = 0.74$ ). The radio source is extended over 1.2 arcsec and overlies the nuclear region of an  $I = 19.9$  mag disc galaxy at a redshift of 0.410 (Cohen et al. 2000). It is detected by *ISO* with  $S_{15\mu\text{m}} = 341 \mu\text{Jy}$ . There is a faint *Chandra* counterpart.

**J123651+621221** (Starburst + AGN?): has a steep spectrum ( $\alpha > 0.71$ ). The MERLIN+VLA image shows a source extended over  $\sim 1.2$  arcsec with no evidence for any compact component. Garrett et al. (2001) also find no evidence for any compact component with the EVN at an angular resolution of 20 mas. The radio structure thus favours a starburst rather than an AGN interpretation. The radio source is identified with very faint emission ( $I > 28$  mag) on the HDF frame. Dickinson et al. (2000) and Dickinson (2000) report a very red object ( $I_{\text{AB}} = 27.8$  mag,  $J_{110} - H_{160} = 1.6$ ) at the position of this source from NICMOS observations, implying a dust-obscured starburst system at a redshift approaching 3. The source is detected by *ISO* with  $S_{15\mu\text{m}} = 48 \mu\text{Jy}$ . Hornschemeier et al. (2001) find a hard X-ray detection with *Chandra* suggesting an obscured QSO at a redshift of 2.7.

The bright ( $I = 21$  mag) galaxy lying 1.5 arcsec to the south is at a redshift of 0.401 (Cohen et al. 2000), and is not thought to be related to the radio source.

**J123652+621444** (AGN): has an inverted spectrum ( $\alpha = -0.12$ ) (Richards et al. 1998) and is observed to vary in intensity on the time scale of months, suggesting the presence of an AGN (Richards 2000). The radio structure shows a compact core and one sided jet-like feature to the east  $\sim 1.3$  arcsec in length. The low resolution WSRT image of this source (Garrett et al. 2000) shows evidence for low surface-brightness emission extending over  $\sim 30$  arcsec to the east. If this is an extension to the core-jet structure seen in the high resolution MERLIN+VLA image, the jet has an overall extent of  $\sim 100$  kpc. The core overlies the nucleus of an  $I = 18.5$  mag elliptical galaxy on the HDF frame at a redshift of 0.321 (Cowie et al. 2004). It is detected by *Chandra*.

**J123653+621139** (Starburst): has a steep spectrum ( $\alpha > 0.77$ ). The radio structure shows a compact component with a slight ( $\sim 0.3$ -arcsec) extension to the east. The compact component overlies the nucleus of an  $I = 21.9$  mag compact galaxy at a redshift of 1.275 (Cohen et al. 2000). It is also detected by *ISO* at  $15 \mu\text{m}$  with a flux density of 180  $\mu\text{Jy}$ . There is a faint *Chandra* counterpart.

**J123654+621040** (Starburst Candidate): has a steep spectrum ( $\alpha > 1.0$ ) and is extended over approximately 1.5 arcsec; it shows no signs of compact emission at 0.2-arcsec resolution. The source lies close to the edge of the

HFF frame but there is no optical identification at the radio source position brighter than  $I = 25$  mag.

**J123655+620917** (Unclassified): has a radio spectrum with  $\alpha > 0.55$ . The source contains a compact component associated with the galaxy nucleus and emission extending over 0.6 arcsec. The compact component overlies the nucleus of an  $I = 20.4$  mag galaxy at a redshift of 0.419 (Cowie et al. 2004)

**J123655+620808** (Unclassified): has a steep radio spectrum ( $\alpha > 0.85$ ) and shows a compact component with emission extending over 0.7 arcsec. The radio source lies outside the CFHT image so no optical frame is shown in Fig. C1. However Cowie et al. (2004) catalogue an  $R = 22.6$  mag galaxy at the position of the radio source with a redshift of 0.792. There is a faint *Chandra* counterpart.

**J123656+621207** (Starburst Candidate): has a steep spectrum ( $\alpha > 1.32$ ), is extended over  $\sim 1$  arcsec and shows no sign of any compact emission at 0.2-arcsec resolution. It lies close to the edge of an HDF frame and at the radio position there is no optical object brighter than  $I = 28$  mag. Richards et al. (1999) report that NICMOS imaging shows no counterpart to the limits  $J > 25$  and  $H > 25$ ; Barger et al. (1999) find no counterpart at  $K > 24$ . The radio source is located  $\sim 3$  arcsec from the second brightest SCUBA source, HDF850.2 (Hughes et al. 1998), but the association is uncertain – see the detailed discussion in Section 8.4.2.

**J123656+621301** (Starburst): has a steep radio spectrum ( $\alpha > 1.22$ ), is extended over 1.2 arcsec and is identified with an  $I = 22.5$  mag compact galaxy at a redshift of 0.474 (Bauer et al. 2002). It has an *ISO* counterpart and is detected by *Chandra*. The bright companion galaxy to the SE has a redshift of 0.475 (Cohen et al. 2000).

**J123659+621449** (Starburst Candidate): is extended over 1.0 arcsec and shows no sign of compact emission at 0.2-arcsec resolution. The radio structure overlies a disturbed  $I = 20.9$  mag disc galaxy at a redshift of 0.761 (Cowie et al. 2004). The galaxy appears to show a dust-lane or double nucleus and may be undergoing a merger. The source is detected by *ISO* and has a faint *Chandra* counterpart.

**J123700+620909** (AGN Candidate): has a steep radio spectrum ( $\alpha = 0.89$ ). There is a compact component with one-sided emission to the NE; the total angular size of the source being  $\sim 0.4$  arcsec. The radio emission There is no optical counterpart at the radio position to the limit of  $I = 25$  mag in the CFHT frame.

**J123701+621146** (Starburst): has a steep radio spectrum ( $\alpha = 0.67$ ) and is extended over 3 arcsec in the VLA-only image at 2-arcsec resolution (not shown). At 0.5-arcsec resolution some of the outer low surface brightness emission is resolved out, but the central 1.5 arcsec of emission is well imaged and shows no sign of any compact component. There is no optical detection at the radio position on the HFF frame brighter than  $I = 25$  mag. The source is detected by *ISO*. J123701+621146 is the most likely radio counterpart to SCUBA 850.6 (see Section 8.4.5). There is a faint *Chandra* counterpart.

**J123702+621401** (Unclassified): has a steep radio spectrum ( $\alpha > 0.79$ ) and is extended over 3.4 arcsec in the VLA-only image (not shown). At 0.5-arcsec resolution the source shows no sign of any compact component and some of the low surface brightness emission is resolved out. The SE end of the source overlies an  $I = 21.9$  mag galaxy at a

redshift of 1.2463 (Cowie et al. 2004), with a significant fraction of the extended emission lying well outside the confines of the optical galaxy; the latter precludes a straightforward classification as a starburst candidate. It is detected by *ISO*.

**J123704+620755** (Starburst Candidate): is extended over 1 arcsec and shows no sign of any compact component. It is outside the CFHT frame but it is detected by *Chandra*.

**J123705+621153** (Starburst): has a steep spectrum ( $\alpha > 1.27$ ) and is extended over 1.5 arcsec with no evidence for any compact component at 0.2-arcsec resolution. The source is centred on the nuclear region of an  $I = 20.6$  mag face-on spiral galaxy at a redshift of 0.902 (Cowie et al. 2004). The source is detected by *ISO* and has a faint *Chandra* counterpart.

**J123707+621408** (Starburst Candidate): has a relatively flat radio spectrum ( $\alpha = 0.29$ ). The source is extended over 0.9 arcsec and there is no evidence for any compact component. The radio morphology favours a starburst classification and the relatively flat spectrum may be attributed to low-frequency free-free absorption. There is no obvious optical identification on the HFF frame although there does appear to be a faint  $I = 24.9$  mag galaxy at the radio position on the CFHT frame. Chapman et al. (2004b) identify the system as a sub-mm galaxy ( $S_{850} = 4.7 \pm 1.5$  mJy) with a redshift of 2.48. It is detected by *Chandra*.

**J123707+621121** (Starburst Candidate): has a steep radio spectrum ( $\alpha > 0.82$ ). It is extended over 0.6 arcsec and there is no evidence for any compact component. There is a faint  $I = 25$  mag object at the radio source position on the CFHT frame.

**J123708+621056** (Starburst Candidate): has a relatively flat radio spectrum ( $\alpha = 0.35$ ) but there is no evidence for any compact radio component at 0.2-arcsec resolution. The radio spectrum may therefore be due to substantial free-free absorption at 1.4 GHz. The source is extended over 0.7 arcsec and is displaced by  $\sim 0.5$  arcsec from the central region of an  $I = 19.8$  mag edge-on disc galaxy at a redshift of 0.422 (Cowie et al. 2004). This separation is probably real since the registration errors, even towards the edge of the HFF, are substantially lower than 0.5 arcsec. There is a faint *Chandra* counterpart.

**J123709+620837/J123709+620841** (AGN and AGN Candidate): are separated by 4.5 arcsec. J123709+620837 has a flat radio spectrum ( $\alpha = -0.35$ ). J123709+620841 is undetected at 8.4 GHz implying a steeper radio spectrum, although it is difficult to separate these sources in the 8.4-GHz image where the angular resolution is comparable with the source separation. They both have compact cores and faint extended emission. The compact component dominates the radio emission in J123709+620837, which is unambiguously identified as an AGN system with a compact flat-spectrum core. J123709+620841 may also be an AGN system, though this is less clear. Each radio source is identified with a separate galaxy ( $I = 20.4$  and 21.4 mag with redshifts of 0.907 and 0.902 respectively (Cowie et al. 2004); in each case the compact radio component overlies the nucleus of the galaxy. Both sources have *Chandra* counterparts, J123709+620837 has the brighter X-ray emission.

**J123711+621330** (AGN Candidate): has a steep radio spectrum ( $\alpha = 0.69$ ). The source contains a compact radio component with one-sided jet-like emission extending

$\sim 1.2$  arcsec to the east. The compact component is coincident with the brightest part of an  $I = 22.7$  mag galaxy. The optical galaxy is asymmetric in the same sense as the radio structure. Bauer et al. (2002) estimate a photometric redshift of 1.112 for this galaxy. The classification as an AGN candidate is based on the registration of the compact component with the bright optical nucleus together with the asymmetry of the radio structure. The associated X-ray emission detected by *Chandra* is significantly offset by 0.9 arcsec to the east of the radio peak.

**J123711+621325** (Starburst Candidate): has a steep radio spectrum ( $\alpha > 1.16$ ) and extends over 0.8 arcsec and shows no sign of compact emission at 0.2-arcsec resolution. The source is identified with an  $I = 25$  mag galaxy on the CFHT frame. Chapman et al. (2004b) identify the system as a sub-mm galaxy ( $S_{850} = 4.2 \pm 1.3$  mJy) with a redshift of 1.99. There is a faint *Chandra* counterpart.

**J123713+621603** (Starburst Candidate): is extended over 0.9 arcsec with no evidence for any compact radio component at 0.2-arcsec resolution. It is identified with an  $I = 22.8$  mag galaxy on the CFHT frame; the source overlies the nuclear region.

**J123714+621558** (Starburst Candidate): is extended over 1.5 arcsec with no sign of any compact component at 0.2-arcsec resolution. The source is identified with an  $I = 20.8$  mag galaxy on the CFHT frame at a redshift of 0.567 (Cohen et al. 2000).

**J123714+620823** (AGN): has an inverted radio spectrum ( $\alpha = -0.15$ ) and the radio structure is almost unresolved. The image shown in Fig. C1 and described in Tables A1 and A2 is from the MERLIN data only. It is identified with the nucleus of an  $I = 22.0$  mag galaxy on the CFHT frame.

**J123716+621512** (AGN Candidate): has a relatively flat radio spectrum ( $\alpha = 0.41$ ). The source consists of a compact component and one-sided emission extending  $\sim 0.4$  arcsec to the south-west. The source overlies the nucleus of an  $I = 19.8$  mag galaxy on the CFHT frame with a redshift of 0.230 (Cowie et al. 2004). There is a faint *Chandra* counterpart.

**J123716+621643** (Starburst Candidate): is extended over 0.9 arcsec. The radio emission overlies what appears to be a pair of merging galaxies on the CFHT frame. The radio emission is offset from the brighter galaxy by  $\sim 1$  arcsec. This is real since the registration errors in this region are  $< 250$  mas. The brighter galaxy has  $I = 21.6$  mag and a redshift of 0.557 (Cohen et al. 2000). There is a faint *Chandra* counterpart.

**J123716+621733** (AGN Candidate): has a steep radio spectrum ( $\alpha > 0.76$ ). The radio structure contains a compact component with a  $\sim 0.6$  arcsec one-sided extension to the S-W. The compact component overlies the nucleus of an  $I = 22.2$  mag galaxy with a redshift of 1.146 (Cowie et al. 2004). It is detected by *Chandra*.

**J123716+621007** (Starburst Candidate): has emission extending over  $\sim 0.7$  arcsec. It overlies the nucleus of an  $I = 19.9$  mag galaxy at a redshift of 0.411 (Cohen et al. 2000). There is a faint *Chandra* counterpart.

**J123717+620827** (Starburst Candidate): has a steep radio spectrum ( $\alpha > 0.77$ ). The radio structure is extended N-S over 2.1 arcsec. At 0.5-arcsec resolution some of the low surface brightness emission is resolved out and there is no

evidence for any compact component. The brightest part of the radio structure overlies the nuclear region of an  $I = 19.7$  mag galaxy on the CFHT frame.

**J123719+620902** (Starburst Candidate): is extended over  $\sim 0.7$  arcsec and overlies the nuclear region of an  $I = 22.1$  mag galaxy on the CFHT frame. This source is not listed in Richards (2000).

**J123721+621129** (AGN): has an inverted spectrum ( $\alpha = -0.28$ ) with a dominant compact radio component and one-sided emission extending  $\sim 0.8$  arcsec to the north. This source is thus almost certainly an AGN system. There is no optical identification at the radio source position brighter than  $I = 25$  mag. There is a distorted disc galaxy to the NE with an estimated photometric redshift of 2.468 (Bauer et al. 2002), but the radio-optical offset of over 1 arcsec is far too high to be accounted for by astrometric errors. Richards et al. (1999) report that from deep  $I$  and  $K$  band imaging (Barger et al. 1999), this radio source is associated with a very red object with ( $I - K > 5.2$ ). There is a faint *Chandra* counterpart.

**J123721+621346** (Starburst Candidate): has a steep radio spectrum ( $\alpha > 0.66$ ). The radio structure is extended over 0.7 arcsec and shows no evidence for any compact component at 0.2-arcsec resolution. The source is identified with an  $I = 22.1$  mag galaxy at a redshift of 1.019 (Cohen et al. 2000).

**J123725+620856** (Unclassified): is extended over  $\sim 0.4$  arcsec. It overlies the nuclear region of an asymmetrical  $I = 22.1$  mag galaxy, with an estimated photometric redshift of 0.984 (Bauer et al. 2002). It is detected by *Chandra*.

**J123725+621005** (Unclassified): is extended over  $\sim 3.8$  arcsec aligned roughly E-W. There is no evidence for any compact component and at 0.2–0.5-arcsec angular resolution some of the low surface brightness emission has been resolved out. The position given in Table A1 is from the VLA-only image (not shown). The radio source overlies the nuclear region of an  $I = 19.1$  mag galaxy with an estimated photometric redshift of 0.360 (Bauer et al. 2002).

**J123725+621128** (AGN – WAT radio galaxy): has a steep radio spectrum ( $\alpha = 1.35$ ). The radio lobes extend over  $\sim 3.8$  arcsec and are oriented E-W. These lobes are characteristic of a classical wide-angled tail (WAT) radio structure. The compact radio core overlies the nucleus of a compact,  $I = 22.9$  mag galaxy and

**J123730+621258** (Unclassified): has a steep spectrum ( $\alpha > 0.79$ ) and contains a compact radio component with extended emission over  $\sim 0.3$  arcsec. The object lies outside the area of the CFHT frame.

**J123732+621012** (Unclassified): is extended over  $\sim 1.9$  arcsec and contains no compact component. The object lies outside the area of the CFHT frame. The position given in Table A1 is from the VLA-only image (not shown).

**J123734+620931** (Unclassified): is extended over  $\sim 2.8$  arcsec and contains no compact component. The object lies outside the area of the CFHT frame. The position given in Table A1 is from the VLA-only image (not shown). There is a faint *Chandra* counterpart.



**Figure C1. The radio structures of the sources in the 10-arcmin field.** The radio images are shown contoured and overlaid on the astrometrically aligned optical fields which are displayed in false colour ( $CI = -1, 1, 2, 3, 4, \dots, 10 \times 10 \mu\text{Jy beam}^{-1}$ ). All coordinates are in J2000 and the leading  $12^{\text{h}}$  and  $+62^\circ$  have been omitted from the Right Ascension and Declination scales respectively. Where no optical field is shown, the region lies outside either the CFHT (Barger et al. 1999), or *HST* WFPC2 images (Williams et al. 1996). The angular resolution of the radio image (in arcsec) is indicated in Table A1 and in the figure together with a hatched beam area. The origin of the optical field shown for each source are given in Table A1.

**Figure C2. The radio emission associated with the SCUBA  $850\mu\text{m}$  sub-mm sources in the HDF.** The combined MERLIN+VLA radio images at the position of each SCUBA sub-mm source in the HDF and HFF (Serjeant et al. 2000) are shown contoured and overlaid on the astrometrically aligned optical field displayed in false colour ( $CI = 1, 1.5, 2, 2.5, 3, 3.5, 4 \times 8.5 \mu\text{Jy beam}^{-1}$ ). All coordinates are in J2000 and the leading  $12^{\text{h}}$  and  $+62^\circ$  have been omitted from the Right Ascension and Declination scales respectively. The  $3\sigma$  SCUBA positional error circle is marked. For HDF850.1, 850.4, 850.5, 850.7, and 850.8 the optical field shown is from the *HST* WFPC2 (Williams et al. 1996). For HDF850.2 the optical field is from the lower angular resolution CFHT (Barger et al. 1999). For HDF850.6 the central pane is from the *HST* and the right centre pane is from the *CFHT*. Borys et al. (2003) list HDF850.4 and HDF850.5 as a single blended source SMMJ123650+621318. The  $1\sigma$  positional error circle for this is marked in blue over HDF850.4.

## APPENDIX C: IMAGES OF RADIO AND SUB-MM SOURCES OVER OPTICAL FIELDS